

CHAPTER 9: AQUEDUCTS – A CASE STUDY

Pietro Croce¹, Maria Luisa Beconcini¹, Martina Muzzi¹, Elisa Rosso¹, Francesca Marsili¹

¹Department of Civil and Industrial Engineering – Structural Division – Univ. of Pisa, Italy

Summary

The Medicean Aqueduct of Pisa (Tuscany, Italy), is a relevant historical infrastructure built at the end of the XVI century, composed of 954 masonry arches over a total length of 6 km. Many of the arches are affected with several decay phenomena, which occurred during the years. These have changed the original static arrangement, so that several arches are collapsed or degraded.

In view of the conservation of this relevant infrastructure, in the present study the procedure provided by the ISO 13822 for the assessment of existing masonry structures is applied; such procedure is a useful tool for the survey of the current state of the building and the resistance of the materials. In particular the present case study shows the importance of the careful observation of the deterioration phenomena for the comprehension of the causes and the possible evolution of the damage mechanisms.

1 INTRODUCTION

The masonry is one of the oldest building materials, so there are many examples of masonry buildings and infrastructures belonging to the artistic and cultural European heritage.

In view of the preservation of their historical, artistic, social and economic values, the assessment of existing masonry structures is an important engineering task in our era, which requires the application of sophisticated analysis methods, based on national building codes and on International Standards, such as ISO 2394, ISO 13822 and ISO 12491, recently developed. In particular, the ISO 13822 provides an useful procedure for the evaluation of existing structures, indicating a method to inquire into the current state of the case study and the resistance of its materials.

The ISO 13822 explains why current standards for structural design are not sufficient for the reliability assessment of existing structures and for the design of their repairs or upgrading. As the ISO 13822 flow chart illustrates, this procedure is characterized by the appraisal of the structures actual reliability, which is reached through a preliminary assessment and, when necessary, by a detailed assessment.

The aim of this research, that has especially been developed in the framework of Leonardo da Vinci Project, is to demonstrate the practical application of the ISO 13822 for the assessment of a relevant historical infrastructure: the Medicean Aqueduct of Pisa (Tuscany, Italy), an arched masonry structure, built at the end of the XVI century.



Figure 1 Panoramic view of the Medicean Aqueduct

The Medicean Aqueduct of Pisa is a case study suitable for the purpose, because many of the arches are affected with several decay phenomena, which occurred during the years, due to ordinary and extraordinary causes. These have changed the original static arrangement, so that several arches are collapsed or degraded.

The goal of this study is to understand how these causes induced the alteration of the original static model. Since the masonry behaves according to a set of specific macro-elements, namely of rigid-bodies, the structural analysis mainly concerns the identification of these macro-elements and the related failure mechanisms activated by specific actions, such as the settlement of foundation or earthquakes.

The structure has been studied with various types of analysis. Since the various aspects of the structural behaviour are captured by different methods, comprehensive answers are obtained only through a combined approach.

The study is organized in accordance with a step-by-step procedure, such as the flow chart of the ISO 13822 (Chapter 6, figure 1) suggests: in the first step the preliminary assessment was performed, considering the available documentation and results from inspection and check; the following step concerns a more detailed appraisal, in which the structural analysis is carried out.

2 PRELIMINARY ASSESSMENT

The purpose of the Preliminary Assessment is a first evaluation of the structural condition using simple methods, such as:

- study of the available documentation;
- preliminary inspection;
- preliminary checks;
- decision on immediate actions;
- recommendations for detailed assessment.

In some case, the outcomes of this first stage could be sufficient to describe by themselves the state of the building and even to arrive to make a diagnosis of the actual damage, but in other cases the conclusion will ask for additional studies and investigations, in order to achieve a more precise and reliable knowledge. Obviously, severe and/or evident crack patterns generally requires deeper investigations.

2.1 Study of available documentation. A brief history

Due to the relevance of this construction, an extensive and important documentation has been found, not only in the State archive in Pisa, but also in the extensive literature about it. Nevertheless, it was also possible to collect some additional interesting information through a local no-profit association '*Salviamo l'Acquedotto Mediceo*' (*Save the Medicean Aqueduct*), specifically devoted to the preservation of the Medicean Aqueduct.

The study of the aforementioned documentation and the comparison of pictures and maps associated to different periods, allowed to deduce the evolution of the Aqueduct during its life, recreating its historical and architectural evolution.

The Medicean Aqueduct is an infrastructure built in 1613 by the Granduke of Tuscany Ferdinando I de' Medici, in order to convey fresh and clean water from Asciano, a small village in the neighbouring of Pisa, to the centre of the town.

This work is constituted by an elevated pipeline, sustained by 954 masonry arches, such as the Roman aqueducts, carrying the water by gravity, and covers a total length of 6 km.

The construction of the aqueduct was framed in a plan of actions originally developed by the Granduke Cosimo I de' Medici - Granduke of Tuscany from 1519 to 1571 - to improve the

hygienic conditions in the town of Pisa. This plan was mainly focused on an hydraulic reorganization of the territory, aimed to guarantee the development and maintenance of strategic communication networks and to recover wetlands, so as to turn them into florid agricultural lands. Further on, this plan allowed the urban renovation of the town by the construction of the Cavalieri Palace and the Medicean Arsenal.

In the original conception, the Medicean Aqueduct was intended to carry water by gravity through an underground pipeline connecting the Spring Valley, near Asciano, to the Pisa town centre, but the difficulties encountered during the excavation as well as the conspicuous water infiltrations, soon persuaded to abandon this design scheme in favour of a more reliable and safe Roman Aqueduct scheme, consisting in an elevated pipeline running on the straight extrados of masonry arches.

The semi-circular masonry arches, spanning generally about 5 meters, are in brick masonry and are sustained by pillars, whose height decreases from the spring to the town.



Figure 2 View of the Medicean Aqueduct, in 1600, during the erection



Figure 3 Historical picture of the Aqueduct

Except the semi-circular arches, the other parts of the structure were built using mixed masonry composed by layers of cut stones intercalated, to regularize the structure, by thin layers of bricks. Finally, to stabilize the construction, transversal buttresses were built every eleven arches.

The water transfer system was composed of three different works: the water collecting and filtering system with the big cistern, the elevated pipeline and the urban distribution networks.

The springing water, duly purified and filtered, was transferred in a big cistern, “*Il cisternone*”, (fig. 4) where it became cleaner since the sediments could deposit. Finally water reached a cabin, from where it was conveyed in the pipeline.



Figure 4 “*Il Cisternone*”, a big cistern for collecting water, in Asciano

The aqueduct, composed by the arches carrying the elevated pipeline, was realized in two different phases: the first one from 1588 to 1594 and the last one from 1610 to 1613. In the first step, the aqueduct was quite completed, so that in 1595 it began to work. During this phase, in the upstream section near to Asciano, several pillars foundations were realized with a system of wooden piles, according to the Vitruvian scheme, due to the swampy ground and the layout of the aqueduct. Finally, in the last section of the aqueduct, the urban distribution network of the water was composed by an underground pipe that conveyed water to the fountains, some of which still in use.

During its construction, the aqueduct began to lean, as a result of the upstream marshland and of design errors, probably in consequence of the undersizing of the foundations, so that already in 1610, few years after its completion, the first rehabilitation works were necessary. Moreover, water was stagnating in the conduit and could not get to Pisa. As a consequence, the upper part of the pipeline was rebuilt in “cotto” and covered with sheets of stone.

Today, the elevated pipe is disused, because of the advanced state of decay: the collapse of several arches and the impending failure of some others.

From upstream to downstream, there is a difference in height of 5.2 meters. The maximum altitude of the pipeline is 7 m above the ground, the total span of each arch is 7 m, the clear span is 5.3 m, and the thickness is 1.2 m about. The dimensions of most of the arches are similar, due to the use of a single timber temporary structure during the construction.

The aqueduct course changes direction in several points (fig. 5.a). Probably the changes in direction aimed also to realize some kind of expansion joints between the various sections of the aqueduct itself, so as to reduce temperature effects. The arches have an *original numbering*, in ascending order from the town centre to upstream, reported in a suitable sign (see, for example, fig. 5.b).

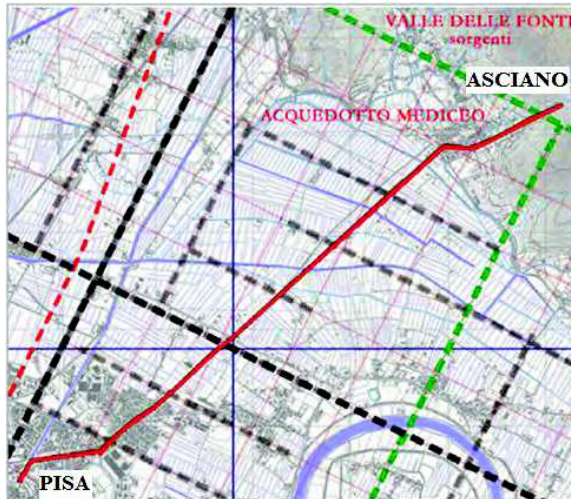


Figure 5.a Aqueduct’s layout

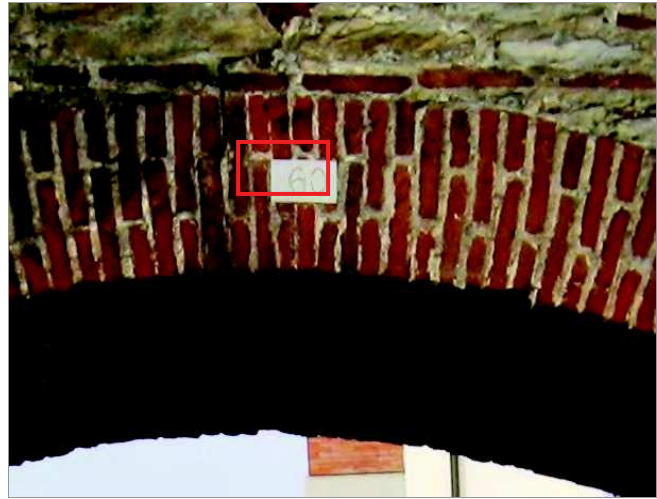


Figure 5.b Original arch sign of the arch nr. 60

The conduit is no longer been used since World War II; a pressurized pipeline has been built underground, following the path of the arches, that allows water to reach the ancient fountains in the city centre (see figs. 6, 7).

2.2 Preliminary inspection

It is useful to analyse separately the phenomena concerned to each structural element, namely:

- the clay pipeline;



Figures 6, 7 Original fountains in Pisa centre: Piazza delle Gondole and Piazza dell'Arcivescovado

- the arches;
- the pillars;
- the buttresses;
- the bases and foundations.

As said, the clay pipeline (fig. 8), with a semi-elliptical section, runs over the arches, covered by a sheet of stone (fig. 9) with protecting function. Nowadays, in the most degraded sections, the sheets of stone are no more in place.



Figure 8 Arch nr. 58, where the core structure and the clay pipeline are visible



Figure 9 The sheet of stone that covers pipeline

As noted, the arches are mainly semi-circular (fig. 10), but in the vicinity of the centre of the town, there are some elliptical arches (fig. 11). There are also some splayed arches (fig. 12): probably this anomaly is an attempt to adjust the arch to the path of the river channels that centuries ago flowed under the aqueduct.

The arches are constituted by brick masonry, 0.45 m thick; the core of the wall is made of stones of irregular shape and size; only some rows of bricks extend throughout the depth of the wall, with regularizing and containing function.

The pillars are of different types, both in size and materials (figs. 13, 14 and 15): stone masonry, mixed masonry, brick masonry, etc. The pillars have a rectangular section, usually 1.8 m long and 1.2 m thick. The pillars of the upstream part of the aqueduct, which support the highest arches, have a larger base, in order to distribute the greater weight on a wider area.



Figure 10 Semi-circular arch (arch nr. 98)



Figure 11 Elliptical arch (nr. 28)



Figure 12 Splayed arch(nr. 29)



Figure 13 Pillar between arches nr.131 and nr. 132



Figure 14 Pillar between arches nr.837 and 838



Figure 15 Pillar between arches nr. 815 and nr.816

The buttresses, which were originally inserted every 11 arches, on both sides of the pillar, in order to contrast the out of plane overturning, differ in size and materials: those located upstream are made of bricks, while the others are made of stones, with the same wall texture of the pillars (figures 16 and 17). The buttresses have a height slightly lower than the pillars, variable according to the corresponding arch; the sloping is about 15 degrees.



Figure 16 Buttress between arches nr. 89-90



Figure 17 Buttress between arches nr. 199-200

The foundation soil of the aqueduct has very poor characteristics, similarly to other sites in and around Pisa. The first information about the foundations have been derived from the

existing literature. Upstream the soil is marshy, so that pile foundations were employed, made of pine logs.

According to the practice of construction, typical of that area and time, we assumed that timber piles have variable length from 6 to 10 m (fig. 18). Approaching the centre of the town, the soil becomes more resistant, therefore the pillars have no pile foundation but a large base which gradually becomes wider (figures 19 and 20).

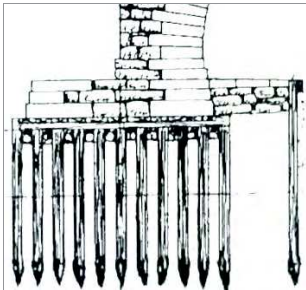


Figure 18 Example of foundation piles, according to the precepts of Vitruvius

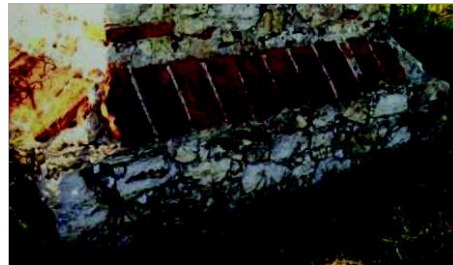


Figure 19 Large base under the pillar, between arches nr. 502-503



Figure 20 Base under the pillar, between arches n°410-411

2.3 Preliminary checks

In this phase a visual inspection of the structure has been conducted, in order to judge its current condition; special attention has been paid to the critical parts.

Over the years, the aqueduct has been subjected to several modifications due to planning mistakes, changes in water demand and difficulties in the maintenance operations. In particular, some earthquakes caused the collapse of some arches: some of these were rebuilt according to a layout different from the original one; others were shored up to avoid their collapse; in some cases, buttresses were built or rebuilt to reinforce the arcade. Obviously, all these changes had the effect of modify the structural setting of the aqueduct.

Nowadays, the observation of the work shows that it is in very critical condition: some arches are collapsed (fig. 21), other are damaged by vehicles impacts (fig. 22); many of them present various decay phenomena: the most evident are cross cracks and organic patinas, such as moisture stains or efflorescence. Over the years some elements, more probably those made almost exclusively in bricks, have been completely or partially rebuilt (figs. 23, 24).



Figure 21 Arch nr. 99, collapsed



Figure 22 Arch n°162, damaged by vehicles impact



Figure 23 Arch nr. 49, rebuilt in bricks



Figure 24 Pillar of arch nr. 130, rebuilt in bricks

The most degraded arches are in the upstream portion of the aqueduct: many of them have been filled with mixed masonry (fig. 25), often different in quality from the original one. The arches that showed an imminent crisis have been provisionally supported by steel or timber scaffoldings (figs. 26, 27 and 28) in the last 30 years.



Figure 25 Some of the stopped up arches, from nr. 685 to nr. 694



Figure 26 Arches nr. 394 and 395, provisionally supported



Figure 27 Arch nr. 870



Figure 28 Arch nr. 890

2.4 Decision on immediate actions and recommendations for detailed assessment

By the preliminary inspection it has been possible to observe that there are types of cracks located in a recurrent way in specific elements, the formation of which can be attributed to the activation of typical arch mechanisms.

In addition, it must be noted that, during the years, poor maintenance was made over the Aqueduct, so that some arches collapsed, while, in other cases, the interventions were mainly devoted to temporarily tackle the most dangerous situations.

Conclusions of the Preliminary Assessment can be summarized as follows:

- the decay occurs with total or partial collapses of arch and with various types of cracks;
- the cracks are probably related to progress of the failure mechanisms;
- several arches in the town centre are unsafe or collapsed, because of vehicle impacts;
- the most damaged arches are those located in the upstream part, which have an evident out of plane inclination;
- the main cause of deterioration is probably the settlement of foundations.

These preliminary results indicate that, for the most critical parts of the structure of the Medicean Aqueduct so identified, further and more detailed inspections are necessary to investigate the real causes of the main decay phenomena, in particular cracks and out of plane rotation of the structure.

Beside the actual damage survey, the evaluation of the original static model of the structure, the knowledge of the actions as well as the evaluation of material properties are key activities to understand the structural behaviour and to arrive to diagnose the actual failure mechanisms and/or crack patterns.

3 DETAILED ASSESSMENT

The detection of the phenomena that led to the damages and the identification of the main causes of observed faults and defects is the first essential step for each safety assessment and for any decision to be taken on possible consolidation of the structure.

Causes of the most relevant degradation phenomena that can be observed in masonry structures can be different, i.e.:

- a) degradation due to the passing of time: deterioration of the material due to endogenous effects (ageing mortar, with progressive decrease in binding capacity; moisture action; plants overgrown) or to exogenous ones (traffic induced vibrations);
- b) the masonry expansion and contraction due to temperature and moisture variation;
- c) the freeze-thaw cycles on the porous walls, which involve swelling and cracking of the masonry; the degradation due to the acid rain; the air pollution effects; the presence of water in the soil which can seep into underground masonry and which can be captured by walls through capillary action;
- d) subsidence, landslide and viscosity, caused by the different soil nature, that involved settlements of foundation;
- e) action of accidental natural forces, such as earthquakes and flooding or by vehicle impacts;
- f) alteration of the original structural scheme through human interventions, such as the insertion of some brick buttresses, the injection of cement mortar inside some cracks, demolition of some arches to help the transit of vehicles on the roads.

Table 1 Typical causes of the most relevant decay phenomena in masonry structures

Variable and environmental actions:	Accidental actions:
a Age dependent effects	e Earthquakes and floods
b Thermal and hygrometric variations	f Human actions (alteration, impacts, etc.)
c Freeze-thaw cycles and atmospheric agents	
d Ground motions	

To better address the subsequent investigations, it is useful to recall that the masonry arch is conceived in such a way to be mainly subject to compression: this is obtained when the arch shape (the arch axis) follows the line of thrust (“*the antifunicular of permanent loads*”).

Over the centuries, many theories have been developed about the typical failure mechanisms of the arch under vertical loads; among them, particularly relevant are: the theory due to De La Hire and Belidor, that considers the sliding of the central part of the arch, and the one due to Mascheroni, which considers the flexural failure mechanism.

In the De La Hire and Belidor’s arch sliding mechanism (fig. 29), the central part of the arch is considered to behave like a wedge, sliding between smooth frictionless surfaces. In the model, the failure occurs when the central body slides down, while the pillars rotate outwards.

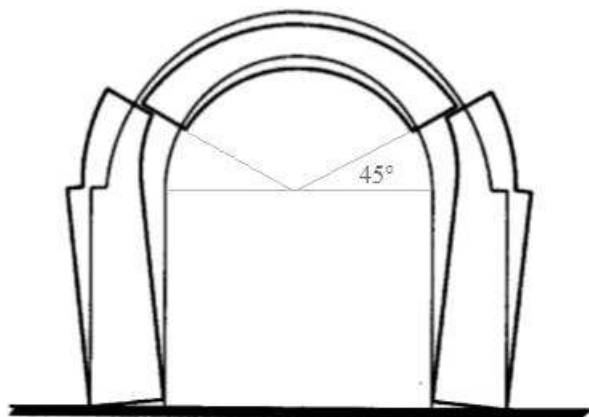


Figure 29 De La Hire and Belidor’s sliding mechanism of the arch

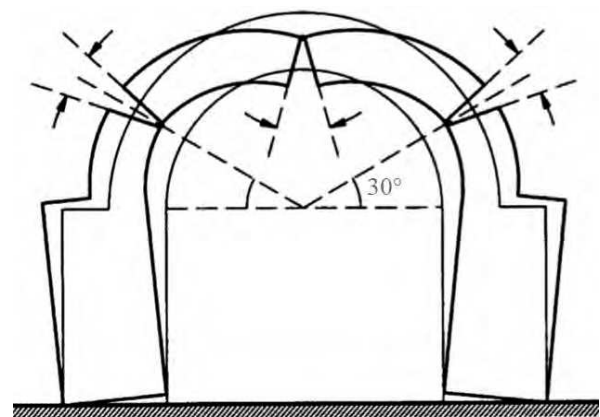


Figure 30 Mascheroni’s flexural failure mechanism of the arch

In Mascheroni’s flexural failure mechanism (fig. 30), the collapse occurs due to the formation of hinges, one at the crown on the extrados and two at the haunches on the intrados, and the rigid rotation of the pillars.

3.1 Detailed documentary search and review of accidental actions

Over the years the aqueduct has been subjected to some accidental events, which altered its structural behaviour.

Probably, the most relevant documented events are two important earthquakes that occurred in the area, probably affecting the stability of the arches. The first one occurred in 1846 with epicenter in Orciano Pisano (fig. 31), of Magnitude 5.6; the second one in 1920, epicenter in Garfagnana (fig. 32), of Magnitude 6.5.



Figure 31 Earthquake with epicenter in Orciano Pisano (5.6 M)



Figure 32 Earthquake with epicenter in Garfagnana (6.5 M)

3.2 Detailed inspection

A careful judgment of the structural condition can be made through specific inspections. Typically, also in ISO 13822, the assessment is a cyclic process. In order to gain a better knowledge of the actual structural condition (particularly in case of damaged structures) and to verify information required for determination of the characteristics and representative values of all basic variables, the first inspection must be often supplemented by subsequent investigation.

The investigation procedure aims to identify:

- the actual state of the structure as well as the crack pattern;
- types, characteristics and mechanical properties of structural materials and soils;
- actions acting on the structure, including environmental effects and accidental actions.

3.2.1 Deteriorations and cracks classification

As seen during the preliminary inspection, the Medicean Aqueduct is subjected to damage that can manifest as deterioration, crack patterns and even partial collapse of arches, depending on the severity of the causes. The careful recording of the decay phenomena during the *in situ* investigations, is the basis for a precise diagnosis of deterioration causes. Therefore, the main deterioration phenomena have been classified, according to the type and the position (see table 2).

Cracks located in the mortar joints are the outcome of tensile stress patterns in masonry elements. Those which are extended on the whole depth of the wall section are identified as *cross cracks*, the others are identified as *not cross cracks*. In addition, both can be further classified according to their position on the masonry wall.

Cross cracks (class A) may be located in the voussoir of the arch, typically at the crown (A2) or at the haunches (A1), and are linked with the opening of hinges, following the Mascheroni's classical failure mode. Other *cross cracks* can be located in the backfill of the arch, following horizontal (A3) or vertical paths (A4); in other cases, they are associated with a

relative displacement in the mortar joint plane (class G). *Not cross cracks* (class B) are often not visible on the intrados; they are classified in analogy to those of class A, with reference to the position and the direction (B1-B2-B3-B4). It is quite frequent to observe the detachment of the arch from the backfill (class E) and/or deterioration phenomena of some masonry elements (class F). Other types of damage are caused by settlement of foundations (class C), which occur with out of plane rotation (C1) or with vertical displacement of the pillar and horizontal cracks in the backfill of the arch (C2). Sometimes, the simultaneous presence of cross cracks and settlement can cause the displacement of a voussoir along the mortar joint (class G). During the years, the concurrence of several cracks in the same arch could activate failure mechanisms (class D), involving the partial collapse of the arch elements -arch crown, masonry backfill, buttress- (D1), or even the collapse of the whole arch (D2).

The considered classes, listed in tab.2, are illustrated by representative pictures in figs. 33 to 39.

Table 2 Types of deterioration

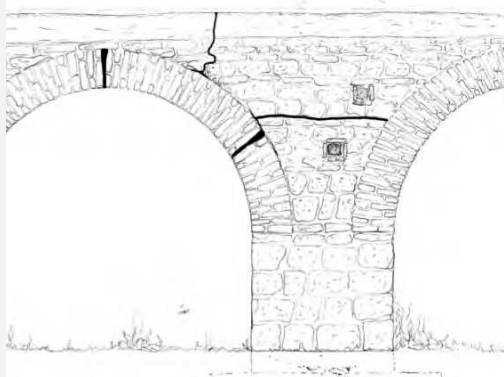
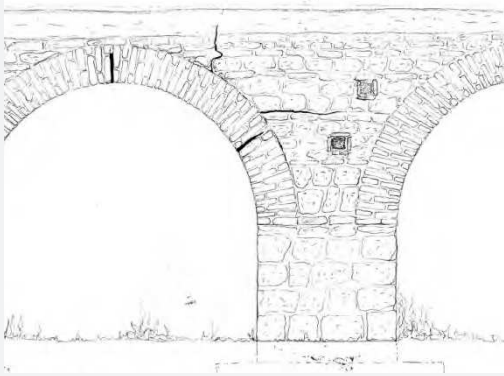
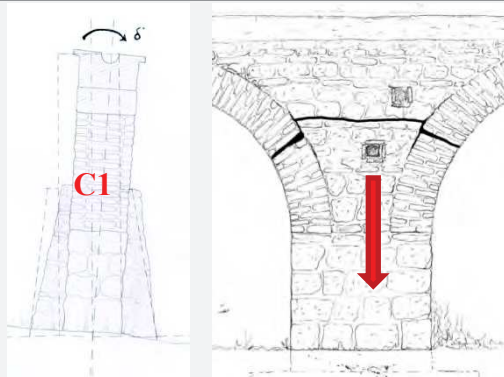
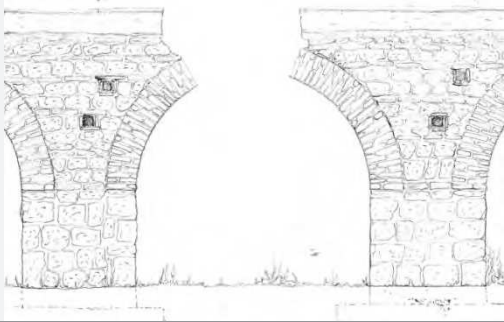
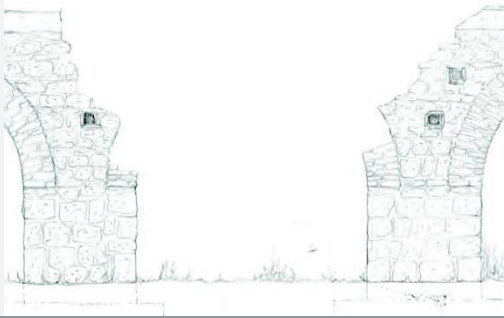
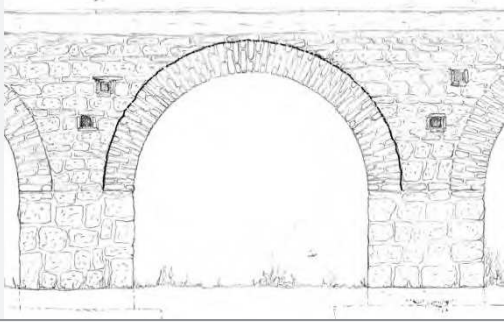
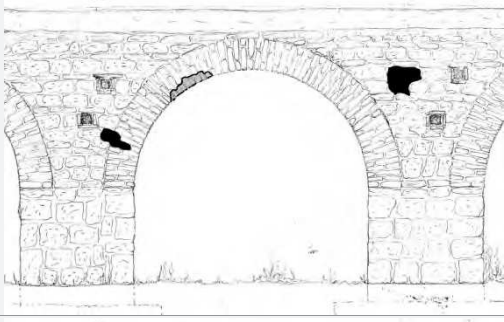
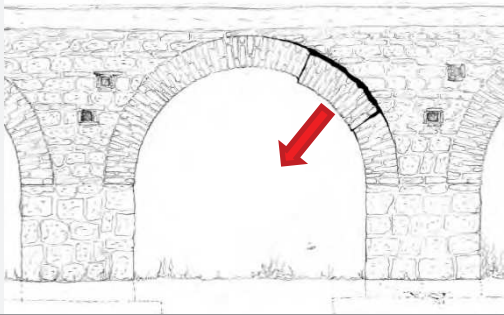
CLASS	GRAPHIC SCHEMES	DESCRIPTION	TAG
(A) CROSS CRACKS		Cracks at the haunch, visible on the arch's bricks and extended through the whole depth	A1
		Cracks at the crown, visible on the arch's bricks and extended through the whole depth	A2
		Horizontal cracks visible on the masonry wall (backfill) and extended through the whole depth	A3
		Vertical or oblique cracks, visible on the masonry wall (backfill) and extended through the whole depth	A4
(B) NOT CROSS CRACKS		Cracks on the voussoir, visible on the arch's bricks but not extended through the whole depth	B1
		Cracks at the crown, visible on the arch's bricks but not extended through the whole depth	B2
		Horizontal cracks, visible on the masonry wall (backfill) but not extended through the whole depth	B3
		Vertical or oblique cracks, visible on the masonry wall (backfill) but not extended through the whole depth	B4
(C) SETTLEMENTS		Settlement of foundation that involves an out of plane rotation of the pillar's foot	C1
		Vertical settlement of foundation	C2

Table 2 Types of deterioration (continuation)

(D) COLLAPSE	 A cross-sectional diagram of a stone archway. The central part of the arch is missing, and the remaining stone blocks on either side are shown with jagged, broken edges, indicating a partial collapse.	Partial collapse of arch elements (arch, masonry backfill or buttress) D1
	 A cross-sectional diagram of a stone archway. The entire arch structure is missing, leaving a large, empty rectangular opening between the remaining stone walls on either side.	Total collapse of an arch. D2
(E) DETACHMENT	 A cross-sectional diagram of a stone archway. The arch is shown as a separate, curved structure that has become detached from the surrounding masonry walls, creating a gap between them.	Detachment between the arch and the masonry backfill. E
(F) DETERIORATION	 A cross-sectional diagram of a stone archway. Several individual stone blocks within the arch and the surrounding masonry are shown with irregular, pitted, and eroded surfaces, indicating general deterioration.	Deterioration of masonry elements. F
(G) RELATIVE DISPLACEMENT	 A cross-sectional diagram of a stone archway. A red arrow points to a specific mortar joint between two stone blocks, where a curved line indicates that the blocks have shifted relative to each other.	Relative displacement along the mortar joint plane. G

A1: crack in the haunch, visible on the arch's bricks and extended through the whole depth



Arch n. 21 – Side A

Extrados crack detail and intrados crack detail



A2: crack in the crown, visible on the arch's bricks and extended through the whole depth



Arch n. 62 – Side A

Extrados crack detail and intrados crack detail



A3: horizontal crack in the masonry wall (backfill)



Arches n. 8, 9 – Side A

Horizontal crack in the backfill

A4: vertical crack in the masonry wall (backfill)



Arch n. 145 – Side B

Vertical cracks in the backfill and in the arch crown

Figure 33 Examples of cross cracks

B1: crack visible on the arch's bricks, placed in the haunch



Arch n. 251 – Side B

Intrados crack detail

B2: crack in the crown, visible on the arch's bricks



Arch n. 211 – Side B

Intrados crack detail

B3: horizontal crack, visible on the masonry wall



Arch n. 17 – Side A

Horizontal crack on the backfill, close to buttress

B4: oblique crack, visible on the masonry wall



Arches n. 101, 102 – Side A

Oblique crack on the backfill and pillar

Figure 34 Examples of not cross cracks

C1: settlement of foundation that involves the out of plane rotation of the pillar



Arch n. 144 – Section
Out of plane rotation (9°) of a pillar between buttresses

C2: vertical settlement of foundation



Arch n. 16, 17 – Side A
Vertical settlement appearing by a crack in the backfill, extended to arch's brick

Figure 35 Examples of settlements of foundations

D1: partial collapse of arch/masonry wall (backfill)



Arch n. 395 – Side A
Partial collapse of arch

D2: total collapse of arch



Arch n. 100 – Side B
Total collapse of the arch

Figure 36 Examples of collapses

E: detachment between the arch and the masonry wall



Arch n. 113 – Side B
Detachment between the arch's bricks and the backfill.



Arch n. 137 – Side A
Detachment of some brick elements from the arch

Figure 37 Examples of detachments

F: deterioration of some masonry elements



Arch n. 163 – Side A
Deterioration of arch's bricks at the extrados and intrados, caused by lorry impact



Arch n. 163 – Side A
Deterioration at the intrados of the arch and deterioration of the façade of the arch

Figure 38 Examples of deterioration of some masonry elements

G: displacement of a voussoir along the mortar joint plan



Arch n. 101 – Side A
Relative displacement in the mortar joint plane



Arch n. 22 – Side A
Relative displacement in the mortar joint plane

Figure 39 Examples of relative displacement along the mortar joint plane

3.2.2 The survey of the Medicean Aqueduct

In order to store the results of the survey, the whole Aqueduct has been subdivided in 9 sections (fig. 40); the original numbering of individual arches, ascending from the town centre towards upstream, has been maintained. The survey has been carried out filling the specific *arch survey form* shown in fig. 41, one for each side, A and B, of every arch. All the collected data, both geometric and related to deterioration, have been collected in summary tables (eg tables 4, 5).

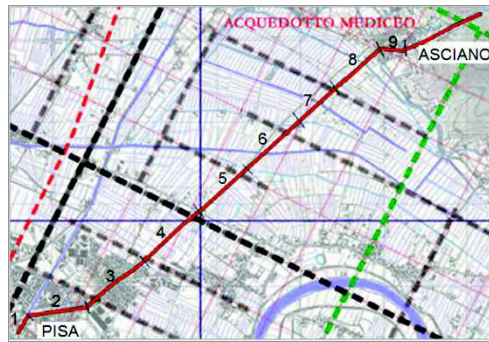


Figure 40 Aqueduct layout divided into 9 sections

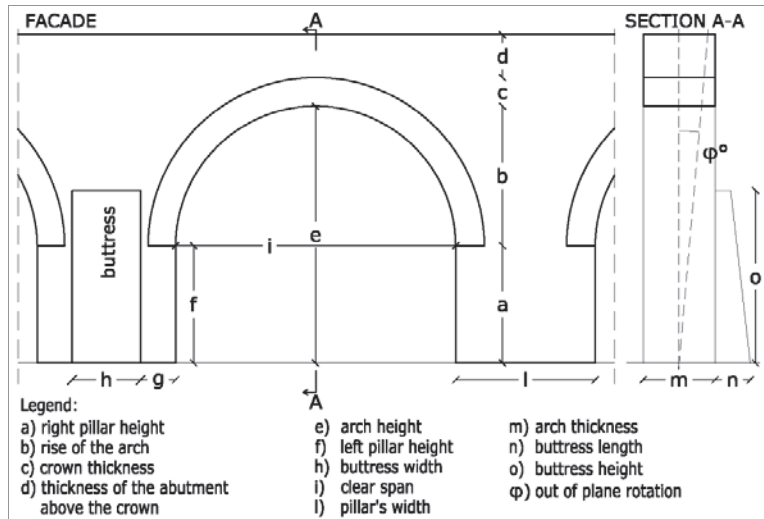


Figure 41 Arch survey form

The investigation of existing crack patterns shows that often several damage phenomena occur simultaneously. For example, the presence of horizontal cracks on a pillar (A3 or B3), on both sides of the arch, is probably associated to vertical settlements of foundation (C2). In this condition, the settlement of one pillar could result in the detachment of the pillar itself from the remaining part, so determining the formation of a new natural arch, spanning between the pillars adjacent to that subject to the settlement, so allowing a new equilibrium configuration, as shown below (fig. 54). The survey on the structure shows that, in some section of the Aqueduct, there are some pillars with an out of plane rotation from 5 to 9 degrees about: for this reason, the following study was carried out also taking account a rotated starting configuration of the structure.

The Medicean Aqueduct also suffers from other decay phenomena such as plants overgrown, that can determine the splitting of stones, moisture and salt efflorescence, which, creeping in the masonry pores, can crumble the materials. If not promptly stopped, these actions can contribute to damage the structure.

4 STRUCTURAL ANALYSIS

A series of structural analyses were conducted on a representative sample of the aqueduct, composed of the 11 arches, placed between two consecutive buttresses.

At first, the studies were conducted on the model of the structure in its original geometry, i.e. in the undamaged state. A preliminary sensitivity analysis was devoted to define the stress patterns under gravitational loads, also accounting for the effects of vertical settlements of foundations and out of plane rotations of the pillars foot. The effects of seismic actions have been investigated, in order to find out the most probable causes of the damages pattern (Global analyses).

Afterwards, in order to identify the failure mechanisms acting on the structure, the effects of seismic actions were investigated on models which describe the actual deformed configuration of the arcades (Local analyses).

In any case, the considered seismic actions are those acting transversely to the mean plane of the aqueduct.

4.1 The case study

For the purposes of the present study, the structural analysis focused on a significant part of the construction, affected by almost all types of decay identified in the classification described above. The sample under investigation consists of eleven arches, placed between two consecutive buttresses, numbered from 90 to 100 (figs. 42, 43), in the section n. 2, next to the town centre of Pisa (fig. 40).

In the following, the product of the survey is illustrated for a relevant portion of the examined sample, corresponding to the three arches numbered 98, 99 and 100 (fig. 44). The cracks, identified by codes accordingly to the classification described above, are highlighted and labelled in different colours. The dimensional data and the crack patterns detected during the survey and previously classified, are summarized in tables 4 and 5. Some other decay phenomena, such as plants overgrown and efflorescence, are evident, but in this case they do not seem to have played a primary role in damaging the structure. For this reason, mainly primary causes have been investigated in assessing the reliability of the structure.



Figure 42 The modelled arches – side A



Figure 43 The modelled arches – side B – side B



Figure 44 Crack pattern of arches n. 98, 99 and 100 – side B

Table 4 Geometric data of arches n. 98, 99 and 100

ARCH	SECTION	GEOMETRIC DATA (m)													
		a	b	c	d	e	f	g	h	i	l	m	n	o	δ
98 A	2	1,99	2,35	0,45	0,45	4,34	2,01	1,80	/	5,32	1,80	1,18	/	/	0°
98 B	2	2,01	2,35	0,45	0,45	4,34	1,99	1,80	/	5,32	1,80	1,18	/	/	0°
99 A	2	COLLAPSED ARCH													
99 B	2														
100 A	2	2,01	2,31	0,45	0,43	4,32	2,05	0,30	1,18	5,30	1,80	1,18	1,07	4,01	0°
100 B	2	2,05	2,31	0,45	0,43	4,32	2,01	1,80	/	5,30	0,30	1,18	1,07	4,01	0°

Table 5 Damages of arches n. 98, 99 and 100

ARCH	SECTION	CROSS CRACK				NOT CROSS CRACK				SETTLEMENT		COLLAPSE		DETACHMENT	DETERIORATION	RELATIVE DISPLACEMENT
		A1	A2	A3	A4	B1	B2	B3	B4	C1	C2	D1	D2	E1	F1	
98 A	2	X	X	X							X			X	X	
98 B	2	X	X			X		X			X			X		
99 A	2											X				
99 B	2											X				
100 A	2	X		X		X								X		X
100 B	2	X			X				X			X		X	X	X

4.2 Characteristics of the models: properties of materials and soil

Since it was not possible to perform direct tests on materials, the mechanical properties were derived from the existing literature related to similar structures, built in the same period and in the same area of the aqueduct.

Almost the whole structure is still composed by the original materials: the masonry of full bricks and lime mortar for the arch crowns, and the mixed masonry in cut stone blocks in all the other parts of the structure. Originally, the employed materials should be of good quality, since they are still in fairly good condition after more than 400 years; so, in the tables contained in the Italian Code [5] (see Annex A), we have referred to good quality materials; in order to take into account the decay due to the age, between the limit values indicated in the table, we have chosen the minimum for the resistances and the medium for the elastic modulus.

The values of the mechanical properties assumed in the analyses are shown in table 6.

Table 6 Mechanical properties of structural materials adopted in the analyses

Type of masonry	Compressive strength f_m [N/mm ²]	Shear strength f_{v0} [N/mm ²]	Elastic modulus [N/mm ²]		Shear modulus G [N/mm ²]	Specific weight W [kN/m ³]
			uncracked condition E	cracked condition E_{cr}		
Cut stone masonry	2,6	0,056	1740	870	580	21
Full brick masonry and lime mortar	2,4	0,060	1500	750	500	18

Unfortunately, direct survey of the existing foundation system is not available, as well as soil testing.

Historical documents testify that, at the construction time, there was a palustrine area at the foot of the mountain. Moreover, in that period, the ground level at the construction site was lower than that of the surrounding plain.

Geological evidences show that the “green” area in Figure 45.a mainly consists of a recent soft alluvial clay layer (2 to 4 m in thickness) overlaying stiffness fan deposit of cobbles. The variable thickness of the shallower soft layer (increasing from upstream to downstream) may be responsible of the observed differential settlements.

The “yellow” areas in Figure 45 mainly consist of outcropping recent silty – sandy alluvial deposits. On the other hand, the “blue” areas mainly consist of clay or peat clay.



Figure 45.a Geographical framework–upstream



Figure 45.b Geographical framework–intermediate section

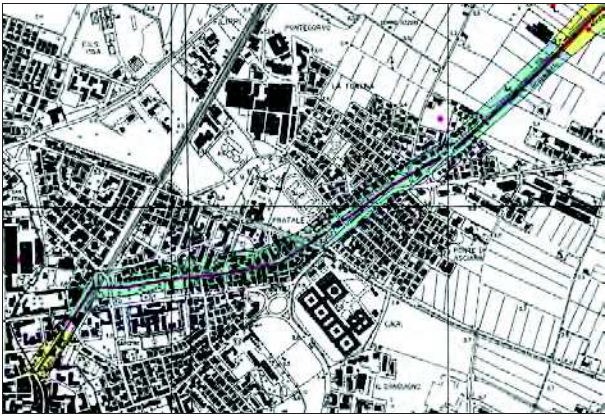


Figure 45.c Geographical framework – downstream section

This area exhibits a shallower layer of vegetable soil of about 0.8 m in thickness overlaying alluvial deposits 3 to 5 m thick with a compressive strength of 200 kPa. A very soft and compressible deposit of clay to peat–clay extends below the alluvial soils. High stratigraphic horizontal heterogeneity of the shallower layers has been observed near the rivers.

4.3 Evaluation of actions

In addition to self-weight, the actions which have been taken into account are:

- vertical settlement of foundation (fig. 46.a), equal to 10, 20, 30 or 40 mm;
- out of plane rotation of a pillar’s foot (fig. 46.b), equal to 1°, 2°, 3° or 4°;
- seismic actions, in terms of response spectrum of the horizontal component of the ground acceleration, evaluated according to the Italian Code [4] (Annex B) for the Service Limit State and the Ultimate Limit State (figs. 47, 48), and of response spectrum of the horizontal displacement for the ULS (fig. 49).

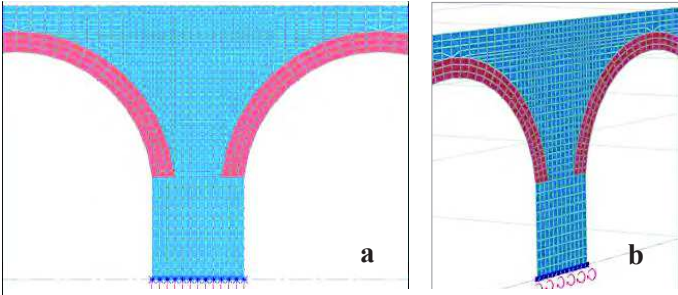


Figure 46.a Vertical settlement of foundation

Figure 46.b Out of plane rotation of pillar’s foot

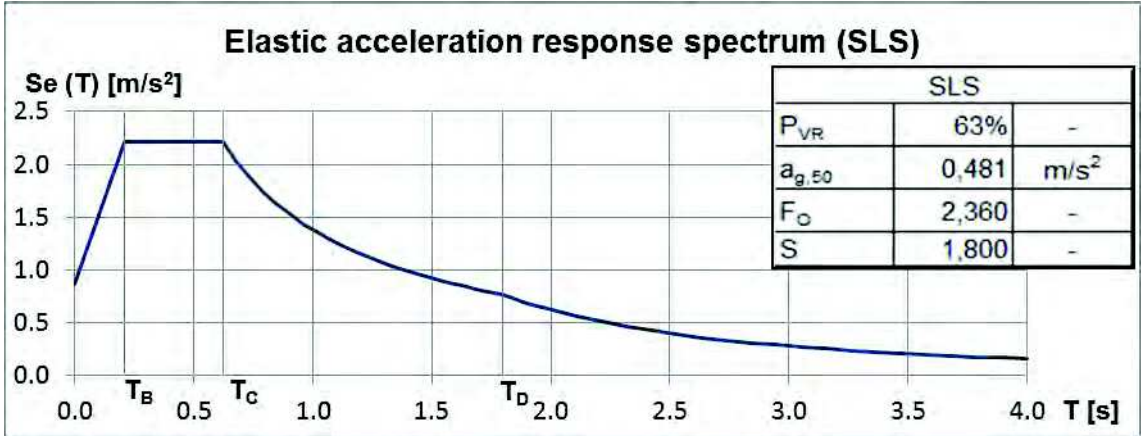


Figure 47 Elastic response spectrum of the horizontal component of the acceleration at SLS

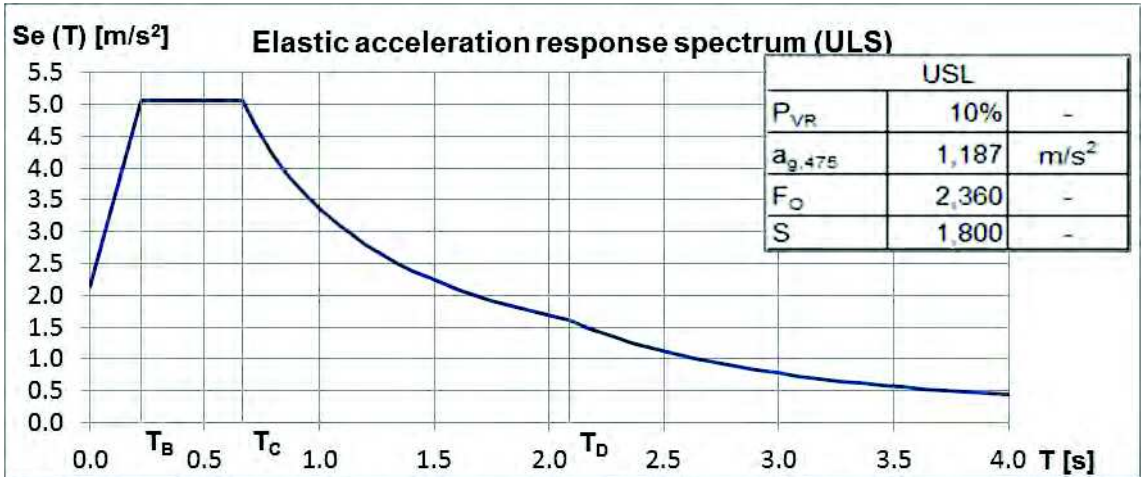


Figure 48 Elastic response spectrum of the horizontal component of the acceleration at ULS

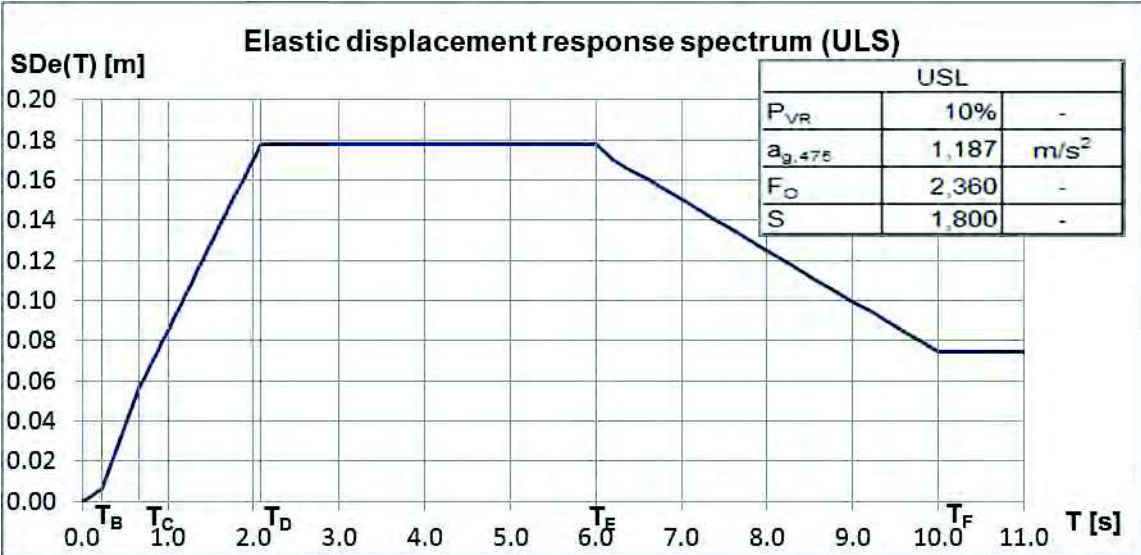


Figure 49. Elastic response spectrum of the horizontal component of the displacement at ULS

4.4 Global analyses

4.4.1 Implemented model

The static and dynamic behaviour of the eleven arches has been numerically studied with a refined *Finite Element Analysis*, performed using the SAP2000 software.

The global finite element model, consisting of about 10299 nodes and 9780 shell elements, is very accurate and it simulates carefully all the details of the modelled arches and buttresses, as well as the soil-foundation interaction. As shown in Figure 50, the model was built with SHELL elements with appropriate thickness; the arches were modelled in the X-Z plane, whereas the buttresses in the orthogonal plane Y-Z.

In order to simulate the soil-structure interaction according to the Winkler model, soil was modelled by a bed of springs with appropriate stiffness. The spring stiffness for vertical movement was defined considering the soil characteristics outlined above. The stiffness to the out-of-plane rotation due to the pillar's thickness was modelled by rotational springs, whose stiffness was evaluated by means of a partial model including a single pillar realized with SOLID elements. In this model, the pillar's foot has vertical springs of equal stiffness; the rotational spring's stiffness is evaluated as the ratio between the moment applied at the top of the pillar and the corresponding rotation.

The stiffness values, assigned to the springs at the foot of the pillars, are shown in table 7.

Table 7 Stiffness assigned to the springs at the foot of the pillars

Spring stiffness for vertical movement	$k_z = 20\,000 \text{ kN/m}^3$
Spring stiffness for the out-of-plane rotation	$k_\theta = 2824 \text{ kN}\cdot\text{m/rad/m}$

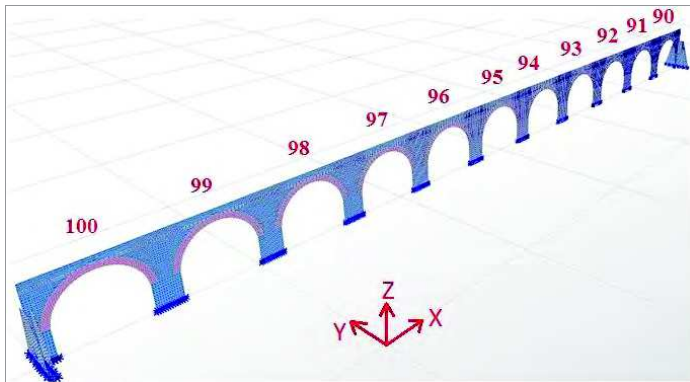


Figure 50.a The finite element model of the eleven arches (shell elements): 3D view

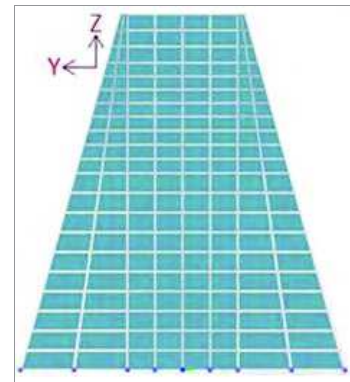


Figure 50.b Finite element model of the buttresses (shell elements) – (Y-Z plane)

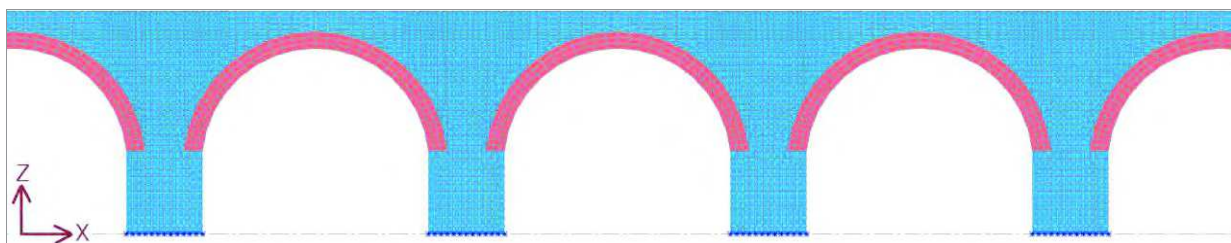


Figure 50.c Finite element mesh of the arches (shell elements) – (X-Z plane)

4.4.2 Static analysis

The static analysis for the self-weight load condition was performed on the global model described above, in the un-cracked situation (elastic modulus = E , see table 6). The results in terms of stresses are shown in fig. 51.

On the same model, vertical settlement of foundation and out of plane rotation of the pillar's foot were imposed alternately on different pillars, to evaluate how the level of stress evolves, on varying of assigned actions: the vertical settlement was applied with an increase of 10 mm at a time, from 0 mm to 40 mm, and the out of plane rotation was applied with an increase of 1° at a time, from 0° to 4° . In fig. 52 the level of stress associated to self-weight and a vertical settlement of 30 mm is shown; in fig. 53, it is shown the level of stress associated to self-weight and an out-of-plane rotation of 4° applied to the pillar's foot.

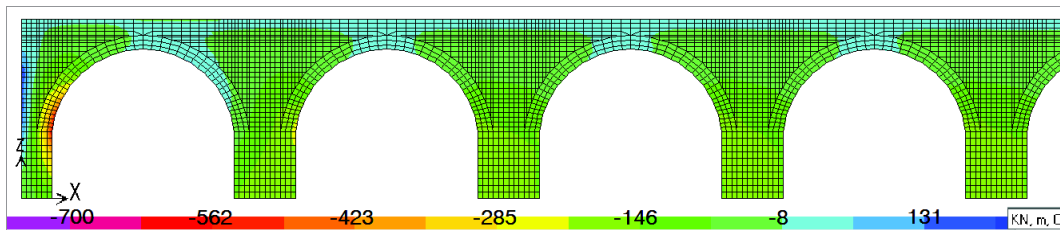


Figure 51 Level of stress, on the shells positive face, along Z direction, in self-weight condition (values expressed in kN/m^2)

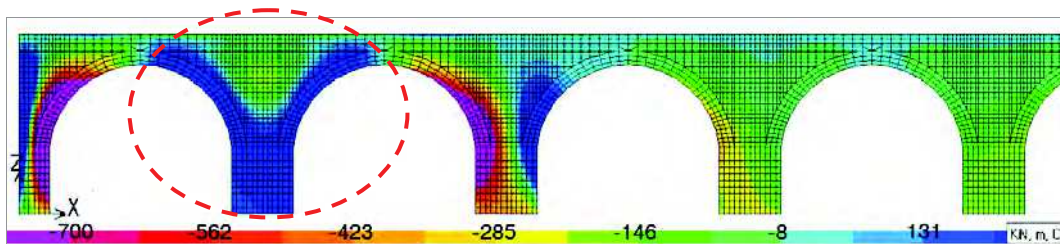


Figure 52 Level of stress, on the shells positive face, along Z direction, self-weight + vertical settlement of 30 mm applied at the foot of the highlighted pillar (values expressed in kN/m^2)

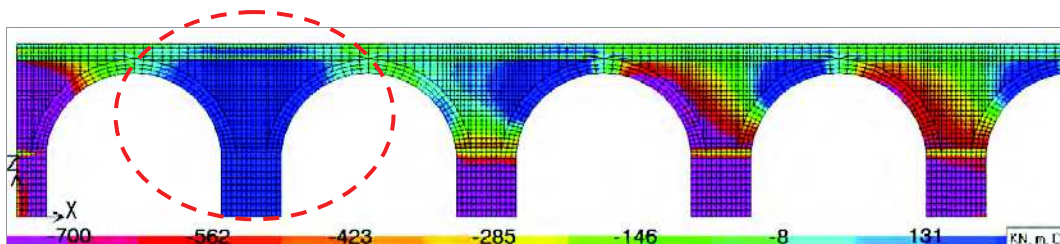


Figure 53 Level of stress, on the shells positive face, along Z direction, self-weight + out-of-plane rotation of 4° applied at the foot of the highlighted pillar (values expressed in kN/m^2)

The figures above show that, while in the self-weight load condition all the structural elements are in compression, when settlement of the pillar foot occurs, tensile stresses appear in that pillar, which values are compatible with the opening of cracks. The distribution of tensile stresses matches with the frequently detected crack pattern, with horizontal cracks on pillars and vertical cracks in the key section of arches, so that we can state that the settlement of foundations is the probable cause of many of the detected crack patterns.

The pattern of stress shown in fig. 52, suggests that, when settlement of foundation occurs, a horizontal cross crack forms in the pillar, and a new mechanism may establish, formed by an arch which includes the two pillars adjacent to the one affected by settlement (fig. 54).

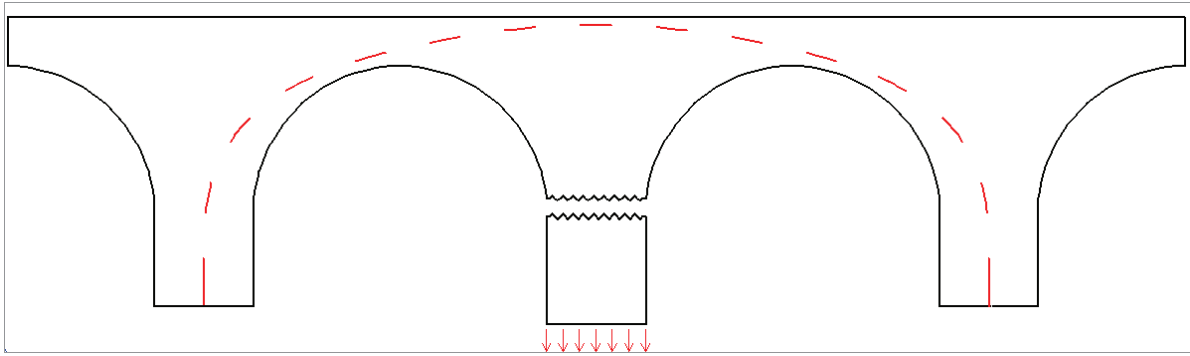


Figure 54 Probable formation of a new mechanism due to the vertical settlement of a pillar

4.4.3 Dynamic analysis

On the global model, both in case of uncracked and cracked conditions, the dynamic modal analysis was performed, obtaining the natural frequencies and the mode shapes of the structure. In figures 55, 56, 57 the first three mode shapes are shown.

The main results can be summarized as follows:

- the first three modes of vibration are in the transversal direction; the corresponding periods are:
 - $T_1 = 1,18 \text{ s}$, $T_2 = 0,88 \text{ s}$, $T_3 = 0,64 \text{ s}$, for uncracked condition (elastic modulus = E);
 - $T_1 = 1,67 \text{ s}$, $T_2 = 1,24 \text{ s}$, $T_3 = 0,91 \text{ s}$, for cracked condition (elastic modulus = E_{cr});
- the participating mass of the first mode of vibration is 78%;
- the first 9 modes of vibration mobilize the mass mainly in the out-of-plane direction;
- 115 modes of vibration are required to reach 95% of participating mass in the transversal direction.

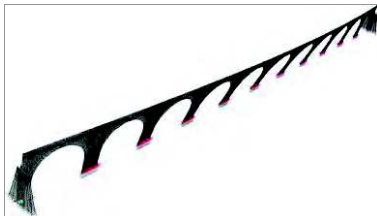


Figure 55 The first mode shape of the structure



Figure 56 The second mode shape of the structure

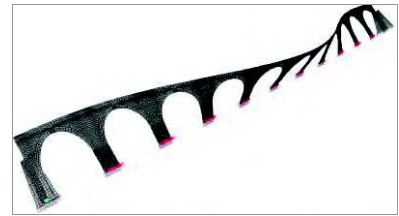


Figure 57 The third mode shape of the structure

4.4.4 Seismic analysis

The verifications for the seismic design situation were performed for the SLS and the ULS in the bottom section of the pillars, where the seismic action is most relevant. The models were those described above, namely that for the uncracked condition (elastic modulus = E) for SLS verifications, and that for the cracked condition (elastic modulus = E_{cr}) for ULS.

For the two limit states, the return periods of the seismic action, according to the Italian Standard [4], are:

- $T_{R,SLS} = 50 \text{ years}$;
- $T_{R,ULS} = 475 \text{ years}$.

The analyses were conducted considering the response spectra shown in figs. 47, 48.

The SLS verification consists in checking the formation of cracks; so the SLS requirement is fulfilled when, in the most stressed sections, the eccentricity of normal force is less than the radius of the inertia central core. The analysis reveals that none of the examined sections satisfies the verification: this means that earthquakes expected with a return period of 50 years probably produce flexural cracking at the bottom of pillars.

The ULS verifications consists in checking the resistance conditions, that is the values of out of plane shear and bending moment do not exceed the design shear strength and bending moment capacity of the section (Annex C). The characteristic values of the strength of the materials are assumed equal to the mean values, shown in table 6.

The analysis shows that the pillars located in the central position are the most stressed; anyway, for the ULS, none of the examined sections of the pillars foot satisfies the above mentioned verifications.

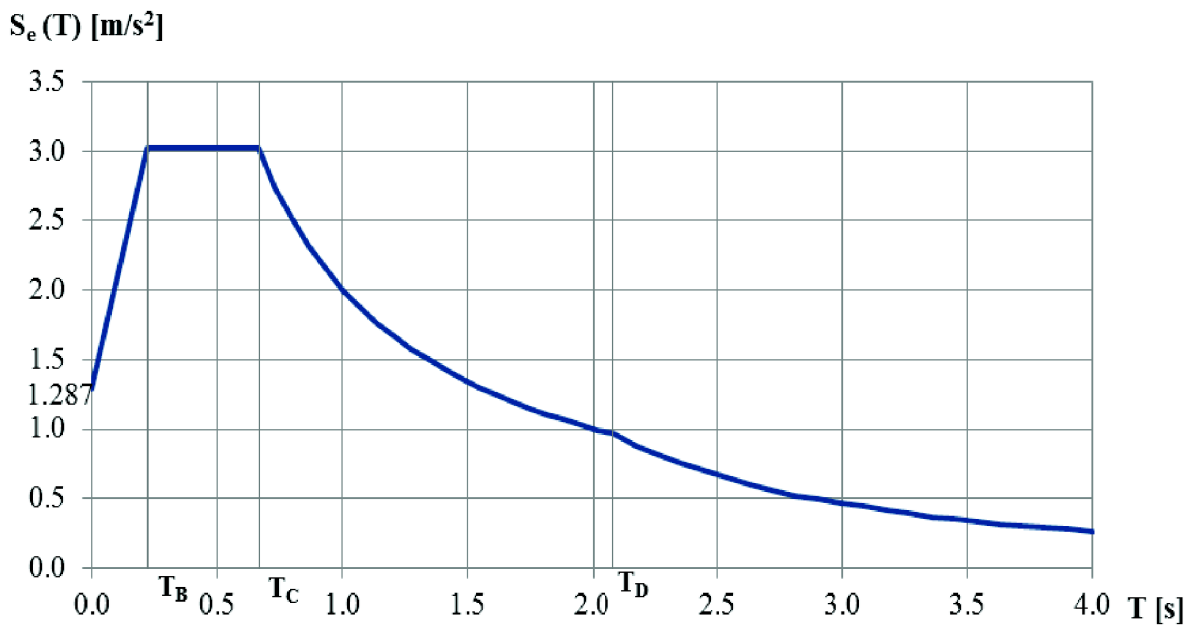


Figure 58 Reduced acceleration response spectrum

Repeating the analysis for reduced acceleration spectra, we found that the verifications were strictly satisfied for the response spectrum shown in fig. 58, corresponding, for the area of interest, to a return period of 140 years. Using such spectrum, a measure of the seismic vulnerability of the structure may be obtained.

The vulnerability index, I_v , may be defined as the ratio between the capacity of the structure and the demand. The capacity of the structure may be expressed by the peak ground acceleration, $a_{g,C}$, in the spectrum compatible with the resistance of the structure, obtained as described above (fig. 58); while the demand is represented by the peak ground acceleration, $a_{g,D}$, in the Standard response spectrum for $T_{R,ULS}$ (fig. 48). So we have:

$$I_{v,a} = \frac{a_{g,C}}{a_{g,D}} \quad (1)$$

For the case study, the vulnerability index is:

$$I_{v,a} = \frac{a_{g,C}}{a_{g,D}} = \frac{1,287}{2,137} = 0,60 \quad (2)$$

4.4.5 Soil-structure interaction and second order effects

The seismic analyses performed with the FEM as described above considers only the elastic behaviour of the structure and of the soil interacting with it, and the verifications apply only to the structure above ground.

In order to take into account the behavior up to failure of the soil interacting with the structure and the second order effects produced by the out-of-plane rotation of the pillars, a specific analysis has been conducted on a limited portion of the examined sample.

The considered portion consists of the central pillar and the two semi-arches on the two sides, isolated from the rest of the arcades; this model does not take into account the stabilizing effect of the buttresses, which is really negligible for the central portions of the sample.

The studied element is considered as a deformable body, connected with its foundation and interacting with soil, in the sense that its base can move vertically and rotate, following the deformation of the underlying soil.

The geometric characteristics of the system are illustrated in fig. 59. The element and the foundation are subdivided in layers, whose mechanical properties are those indicated in table 6 and illustrated in fig. 60; the soil interacting with the element is modelled by layers of elasto-plastic material, 50 cm thick and with horizontal dimensions increasing with depth; the mechanical characteristics of the layers change with the depth, as indicated in fig. 61, taking properly into account the over-consolidation effect.

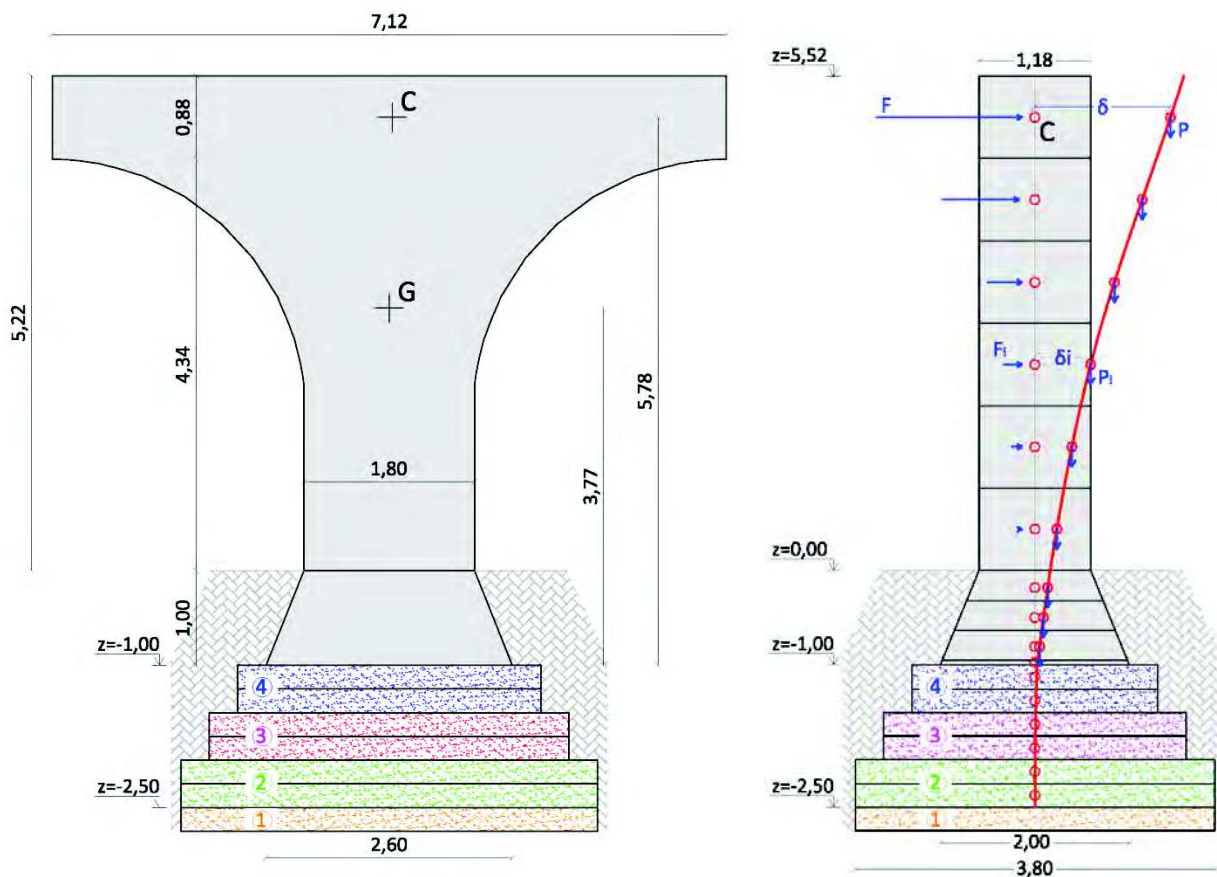


Figure 59 The system element+foundation+soil, modelled as a series of overlapped layers

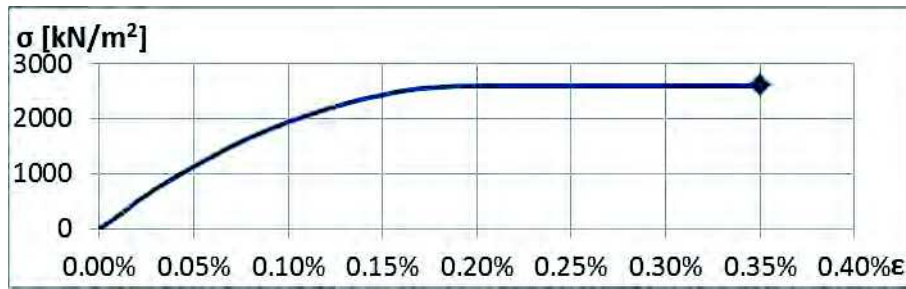


Figure 60 Stress-deformation diagram for masonry

Each layer of the element is subjected to the corresponding self-weight and to a lateral force, F_i , simulating the seismic action; lateral forces are equal to the product of the mass of the layer for its height related to the extrados of the foundation, and for the acceleration of soil, a .

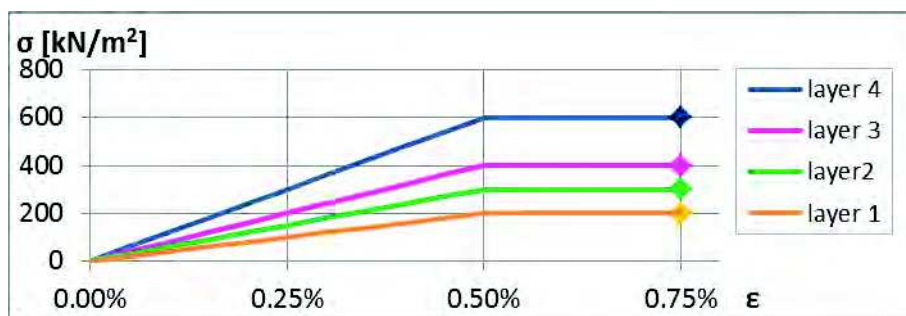


Figure 61 Stress-deformation diagrams for the 4 layers of soil at different depths

The acceleration a is increased by steps; for each step the deformed configuration is evaluated as described in Annex E, taking into account the second order effects too. The procedure stops when in one of the layers the resisting moment is reached.

The result of the procedure is the capacity curve of the system, illustrated in fig. 62, in terms of a , spectral acceleration, and d , displacement of the control point, C.

The failure occurs at the base of the pillar for $a = 1,17 \text{ m/s}^2$. In correspondence, the vulnerability index may be calculated:

$$I_{v,a} = \frac{a_{g,C}}{a_{g,D}} = \frac{1,170}{2,137} = 0,55$$

It can be noted that the seismic vulnerability evaluated taking into account the behaviour of the soil and the second order effect is slightly lower than that in the hypothesis of linear behaviour.

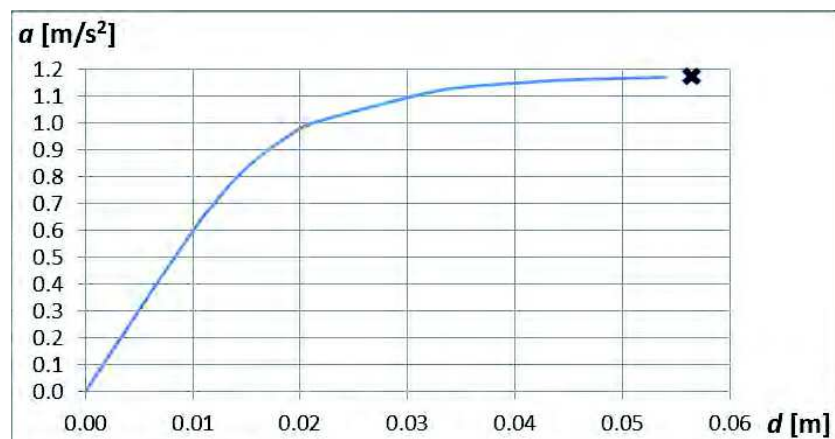


Figure 62 Capacity curve

4.5 Local analyses

The seismic analyses have shown that seismic events with a return period corresponding to the SLS cause the cracking of the sections at the bases of the pillars, and events with a return period of only 140 years induce tensions higher than the flexural strength of those sections.

In structures subjected to seismic actions, in particular masonry structures, the fact that in some sections the strength is exceeded does not imply that the structure or some elements collapse. In many structures, with ductile behaviour, the actions are redistributed among the different elements, and the entire structure may withstand actions much higher. Such structures are usually verified taking into account the post-elastic behaviour, or by means of non-linear analyses or adopting the design spectra, reduced with respect to the response spectra by the behaviour factor, q .

Masonry structural elements do not have a real ductility; however, in complex masonry structures, after the elastic phase, different mechanisms may take place, through which the structure may withstand actions much higher.

In the case study, subjected to seismic actions orthogonal to the main plane, a portion of the structure, separated from the others by the cracks formed for various reasons, may begin to oscillate (activation of the mechanism) and, for stronger actions, overturn (collapse).

This kind of crisis cannot be predicted by the elastic analysis of the structure in the original geometry; in these cases, it is appropriate to recognize the mechanisms that probably establish and evaluate the behaviour of each of them under increasing lateral forces through the so-called kinematic analysis.

The kinematic analysis is based on the kinematic theorem of the limit analysis method: this type of analysis, as well as its main field of application, is fully described in "Annex D".

The first step of the analysis consists in the identification of the conditions which may produce the activation of the local damage or the collapse mechanism. In the structure under examination the probable mechanisms that have been identified take place from the formation of vertical cracks at the key of two arches. There are two extreme situations:

- 1) the cracks form in the arches next to the buttresses (fig. 63.a),
- 2) the cracks form in the arches next to an intermediate pillar (fig. 63.b).



Figure 63.a Mechanism with cracks in the arches next to the buttresses



Figure 63.b Mechanism with cracks in the arches next to an intermediate pillar

In both cases, the macro-element consists of one pillar and the two adjacent semi-arches (highlighted in red in fig. 63.a and fig. 63.b), separate, because of cracks, from the rest of the structure and from the foundation. The characteristics of the macro-element are described in fig. 64.

In situation 1), the central macro-element, which is in the worst situation, is not affected by the stabilizing effect exerted by the buttresses; so, it is subjected to the self-weight and to lateral forces simulating the seismic actions.

In situation 2), a sort of arch effect may develop in the horizontal plane, as illustrated in fig. 63.b, by which the side portions of the arcade transmit stabilizing forces to the macro-element, in correspondence of the arches. So the macro-element is now subjected also to stabilizing horizontal forces, which intensity depends on the out-of-plane position of the arch itself.

The two situations are examined below, for the macro-element modelled as a rigid body rotating around a cylindrical hinge placed at the edge of the pillar's base.

The following cases have been examined:

- case A) macro-element in situation 1), i.e. isolated, subjected to the self-weight and to lateral forces simulating the seismic actions, rotating as a rigid body around a cylindrical hinge placed at the edge of the pillar's base; also the cases of macro-element initially rotated by 5° or 9° have been studied;
- case B) evaluation of the stabilizing forces acting in situation 2);
- case C) macro-element in situation 2), subjected to the self-weight, to lateral forces simulating the seismic actions and to the stabilizing actions (from case B), rotating as a rigid body around a cylindrical hinge placed at the edge of the pillar's base.

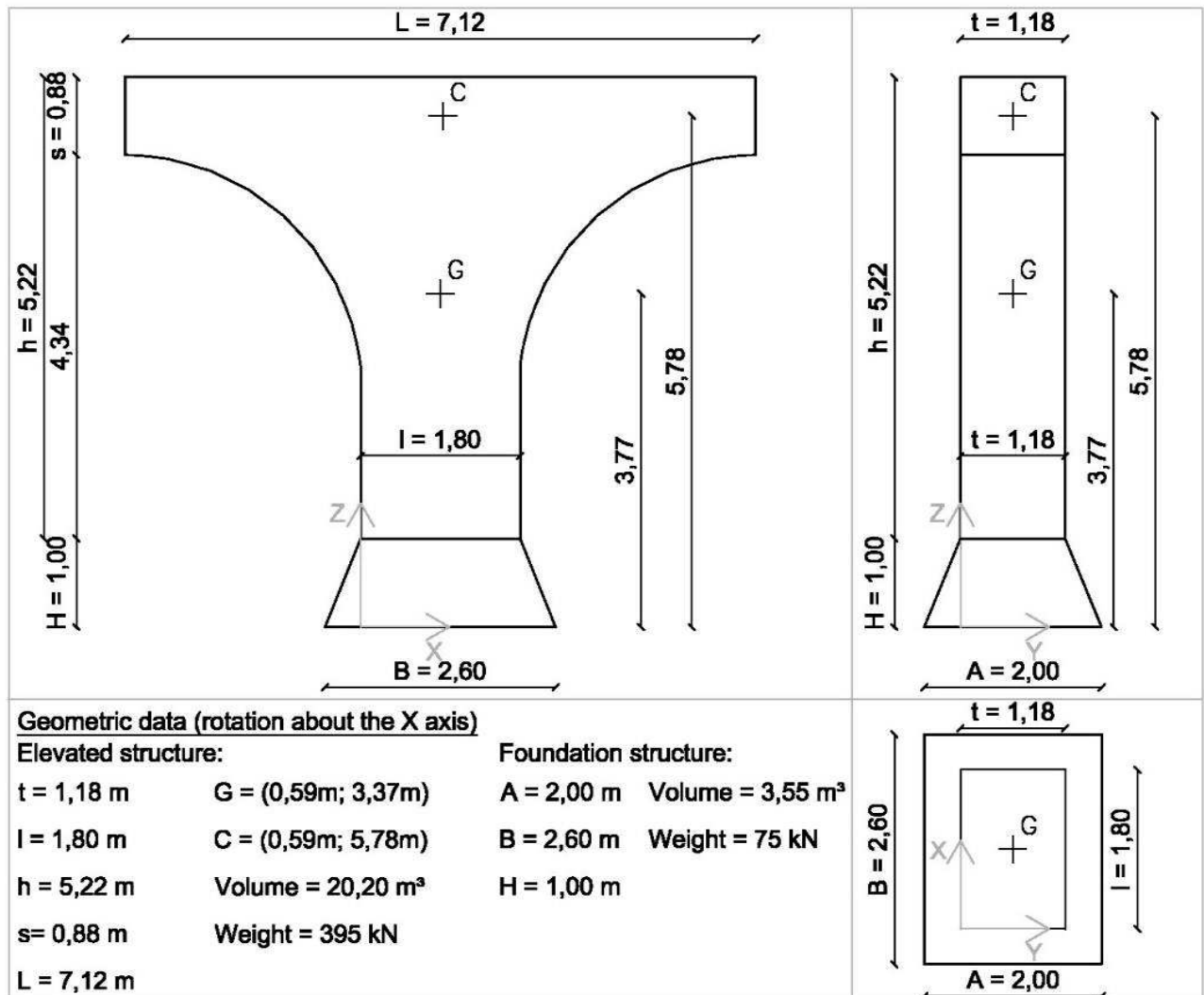


Figure 64 Kinematic Analysis – geometric properties of the macro-element

4.5.1 Case A)

The macro-element is considered as a single degree of freedom rigid body (fig. 65); the seismic actions are modelled as horizontal forces equal to the gravity forces amplified by a kinematic multiplier α . The linear kinematic analysis (see Annex D, §D.3) has been performed to evaluate the kinematic multiplier, α_0 , corresponding to the activation of the mechanism. Afterwards, by means of the non-linear kinematic analysis (see Annex D, §D.4), the displacement capacity of the structure has been determined. Finally, the capacity curves of the structure (see Annex D, §D.5) have been determined and the safety verifications conducted both for the SLS and the ULS (see Annex D, §D.6).

The results of the analysis are shown in table 8 and table 9.

In the tables the symbols indicate:

- φ is the initial rotation of the macro-element
- α_0 is the kinematic multiplier corresponding to the activation of the mechanism
- M^* is the participating mass
- a_0^* is the spectral acceleration corresponding to the activation of the mechanism
- $a_{g,SLS}$ is the acceleration demand related to SLS
- $a_{g,ULS}$ is the acceleration demand related to ULS
- θ_{max} is the rotation corresponding to $\alpha=0$, i.e. to the overturning
- d_0 is the displacement of the control point corresponding to $\alpha=0$
- d_0^* is the spectral displacement corresponding to $\alpha=0$
- d_u^* is the displacement capacity at the ULS
- d_s^*, a_s^*, T_s are the parameters for the calculation of $S_{De}(T_s)$ (see Annex D, §D.6)
- $S_{De}(T_s)$ is the displacement demand at the ULS

In fig. 66, for the element in the three initial conditions, 0° , 5° , 9° , are shown the a^* - d^* curves, the points representing d_u^* , the limit lines representing $a_{g,SLS}$ and $a_{g,ULS}$, and the limit lines representing $S_{De}(T_s)$. It appears clearly that, for the macroelement in the vertical position, the mechanism does not activate for earthquakes corresponding to SLS, for earthquakes corresponding to ULS, the mechanism activates but the element does not collapse; for elements initially inclined 5° the mechanism activates also for earthquakes corresponding to SLS but it does not collapse for ULS earthquakes, while the collapse occurs for macro-elements initially inclined by 9° .

In the case of element initially vertical the index of vulnerability is bigger than 1,00.

Table 8 Results of verifications of the activation of the mechanism

	CAPACITY			DEMAND	VERIFICATION	DEMAND	VERIFICATION
	α_0	M^* [kg]	a_0^* [m/s ²]	SLS $a_{g,SLS}$ [m/s ²]	SLS $a_0^* > a_{g,SLS}$	ULS $a_{g,ULS}$ [m/s ²]	ULS $a_0^* > a_{g,ULS}$
0°	0,174		1,702	0,865	YES	2,137	NO
5°	0,085	43	0,831	0,865	NO	2,137	NO
9°	0,015		0,145	0,865	NO	2,137	NO

Table 9 Results of verifications of collapse

CAPACITY			DEMAND				VERIFICATION ULS	
φ	d_0^* [m]	θ_{max} [°]	d_u^* [m]	d_s^* [m]	a_s^* [m/s ²]	T_s [s]	$S_{De}(T_s)$ [m]	$d_u^* > S_{De}$
0°	0,839		0,336	0,134	1,430	1,925	0,164	YES
5°	0,427	10°	0,171	0,068	0,698	1,964	0,167	YES
9°	0,086		0,034	0,014	0,121	2,110	0,177	NO

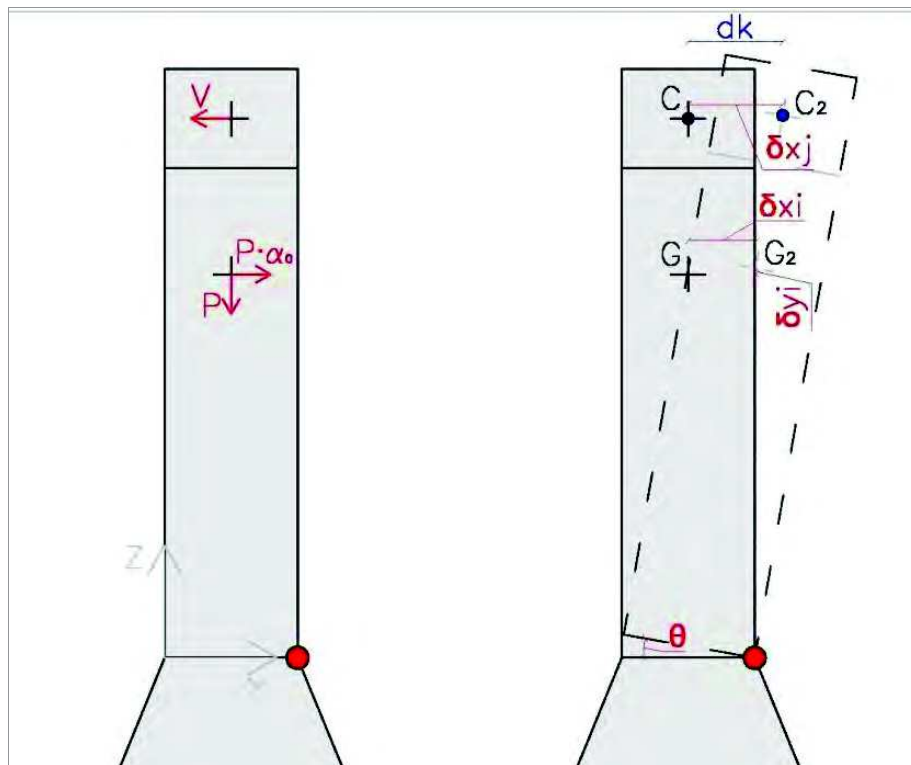


Figure 65 Macro-element as a single degree of freedom body

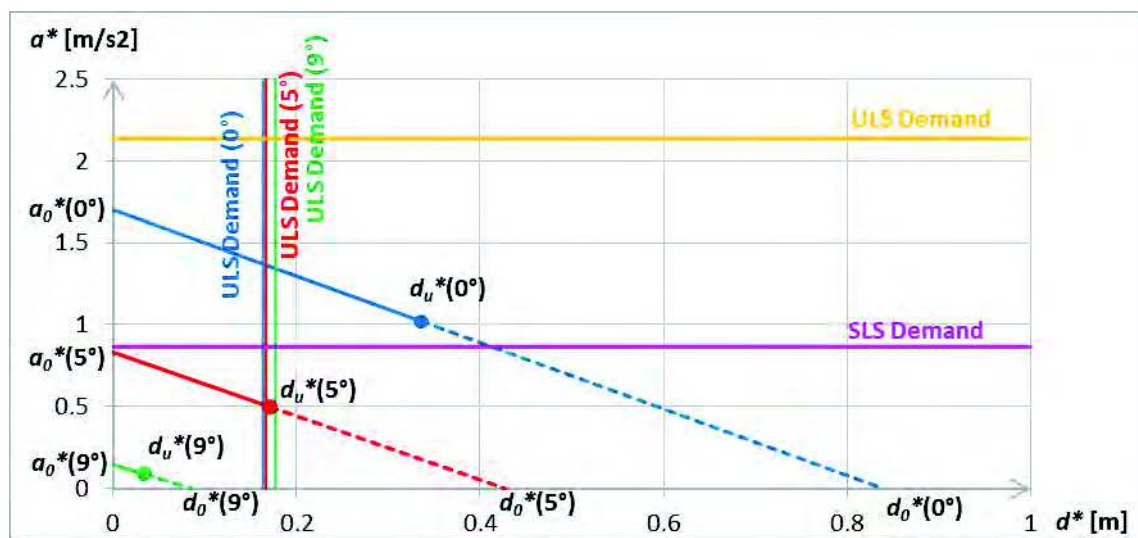


Figure 66 a^* - d^* capacity curves ($\varphi=0^\circ, 5^\circ, 9^\circ$) compared with demand values

4.5.2 Case B): evaluation of the stabilizing forces

In situation 2), shown in fig. 63.b, the out-of-plane rotation of the studied macro-element induces horizontal compressive forces in the upper part of the macro-element itself and in the adjacent ones, due to their geometry, essentially the thickness/length ratio, which is quite high. So, a sort of arch effect may develop in the horizontal plane (fig. F.1 – Annex F), by which the side portions of the arcade transmit stabilizing forces to the macro-element, which intensity depends on the out-of-plane position of the macro-element itself.

The magnitude of the horizontal forces, V , which act on the studied macro-element in opposition to the seismic forces, is a function of the transversal displacement, δ , of the macro-element; it may be evaluated following the procedure described in Annex F. The result for the case under examination is shown in the diagram of fig. 67.

It can be noticed that initially the force V increases from 0 to a maximum, because the tension in the compressed bands increases; after that, the tension no longer increases, while the forces N and H are more and more aligned, so that V decreases up to 0.

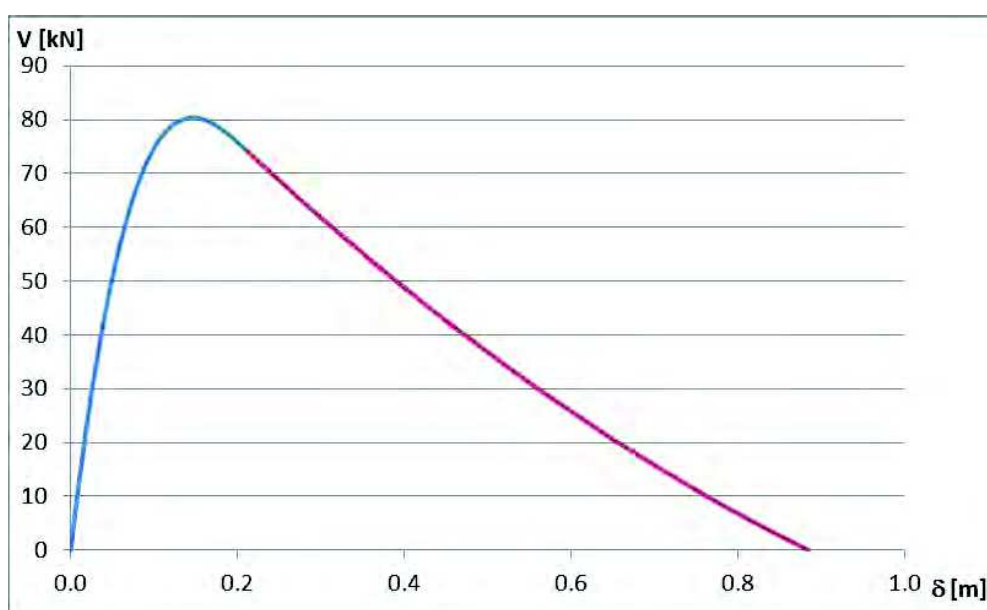


Figure 67 Diagram of V as a function of δ

4.5.3 Case C)

The macro-element is considered as a single degree of freedom rigid body mechanism (fig. 65); the seismic actions are modelled as horizontal forces equal to the gravity forces amplified by a kinematic multiplier α . In this case the horizontal forces, V , act on the studied macro-element in opposition to the seismic forces.

The linear kinematic analysis (see Annex D, §D.3) has been performed to evaluate the kinematic multiplier, α_0 , corresponding to the activation of the mechanism. Afterwards, by means of the non-linear kinematic analysis (see Annex D, §D.4), the displacement capacity of the structure has been determined. Finally, the capacity curves of the structure (see Annex D, §D.5) have been determined and the safety verifications conducted both for the SLS and the ULS (see Annex D, §D.6). The results of the analysis are shown in table 10 and table 11.

In fig. 68, for the element in the three initial conditions, 0° , 5° , 9° , are shown the a^* - d^* curves, the points representing d_u^* , the limit lines representing $a_{g,SLS}$ and $a_{g,ULS}$, and the limit lines representing $S_{De}(T_s)$.

It appears clearly that, for the macro-element in the vertical position, the mechanism does activate for earthquakes corresponding to ULS but the element is much more stable than in the

case A) since the acceleration must still increase to induce greater displacements. Also in this case the vulnerability index is greater than 1,00.

For the element initially inclined 5° the situation is sensibly safer than in case A), with vulnerability index greater than 1,00. Only the element inclined 9° is still vulnerable, and this is logic, considering that even in absence of lateral forces it is at the point of overturning (10°).

Table 10 Results of verifications of the activation of the mechanism

φ	CAPACITY		DEMAND SLS		VERIFICATION SLS	DEMAND ULS		VERIFICATION ULS
	α_0	M^* [kg]	a_0^* [m/s ²]	$a_{g,SLS}$ [m/s ²]	$a_0^* > a_{g,SLS}$	$a_{g,ULS}$ [m/s ²]	$a_0^* > a_{g,ULS}$	
0°	0,174		1,702	0,865	YES	2,137	NO	
5°	0,392	43,276	3,845	0,865	YES	2,137	YES	
9°	0,084		0,825	0,865	NO	2,137	NO	

Table 11 Results of verifications of collapse

φ	CAPACITY			DEMAND				VERIFICATION ULS
	d_0^* [m]	θ_{max} [°]	d_u^* [m]	d_s^* [m]	a_s^* [m/s ²]	T_s [s]	$S_{De}(T_s)$ [m]	$d_u^* > S_{De}$
0°	0,889		0,356	0,142	1,430	1,982	0,168	YES
5°	0,471	10,6	0,188	0,075	3,230	0,959	0,081	YES
9°	0,134		0,054	0,021	0,693	1,106	0,094	NO

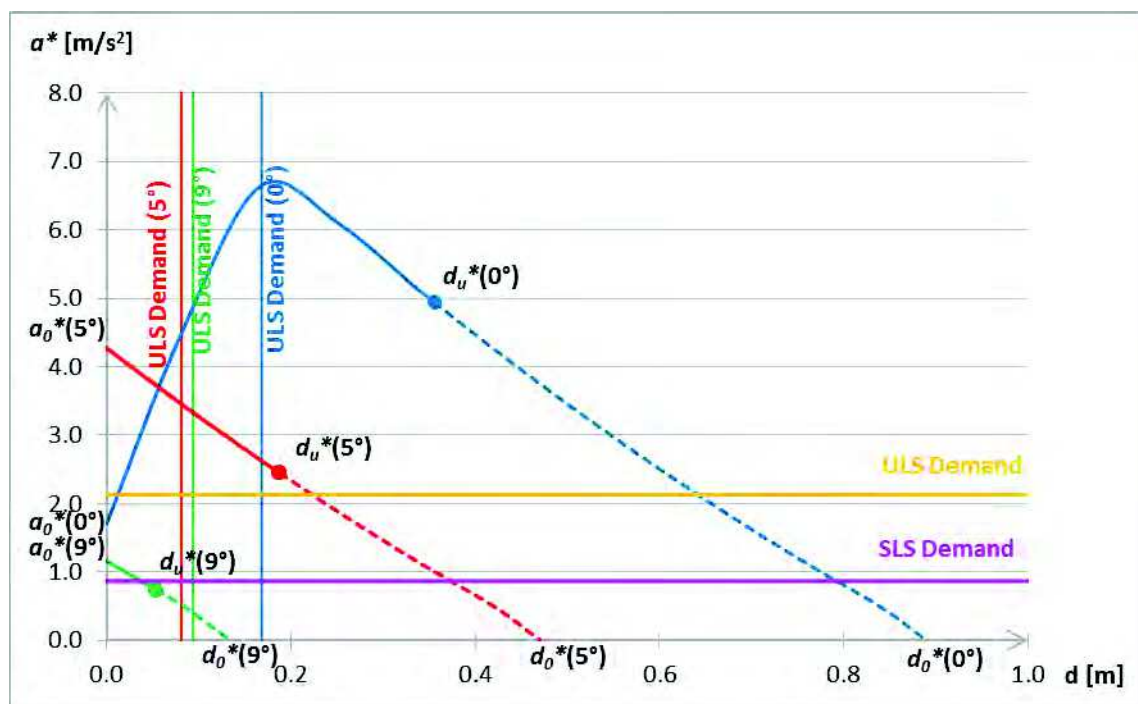


Figure 68 a^* - d^* capacity curves ($\varphi=0^\circ, 5^\circ, 9^\circ$) compared with demand values

5 CONCLUSIONS

The Medicean Aqueduct is an infrastructure which strongly characterizes the territory of the town of Pisa (Tuscany, Italy), for its historical and architectural value.

The Aqueduct was built at the end of the XVI century and just from the beginning it had structural problems, caused by design and construction defects, so that changes and consolidation have been implemented through time. Despite all, the construction is still standing, and, although not working and deteriorated, it is an important monument that must be preserved.

Every consolidation design must be preceded by an accurate analysis, both historical and structural, so that the intervention will be well calibrated for the specific situation.

For the Aqueduct, the procedure outlined by the ISO 13822 has been followed: on the basis of an accurate assessment of the geometry, the materials and the decay, refined models have been implemented in order to justify the main cracks, rotations and collapse observed.

Afterwards, seismic analyses have been conducted, both on global and local models, also taking into account the interaction with soil and the second order effects; the vulnerability of the structure has been obtained and also indications useful for the design of consolidation works.

The methodology followed in the present work has proved to be a useful tool for the study of historical constructions, in view of their conservation.

REFERENCES

- [1] ISO 12491 “Statistical methods for quality control of building materials and components”, 1st edition, 1997.
- [2] ISO 2394 “General principles on reliability for structures”, 1998.
- [3] ISO 13822 “Basis for design of structures - Assessment of existing structures”, 2001. ISO, Geneva, Switzerland.
- [4] *D.M. 14 gennaio 2008* Norme Tecniche per le Costruzioni, Italian Standard.
- [5] *Circ. n° 617, 02 febbraio 2009*, Italian Standard.
- [6] EN 1998-1 (2004): Eurocode 8: Design of structures for earthquake resistance – Part 1: General rules, seismic actions and rules for buildings [Authority: The European Union Per Regulation 305/2011, Directive 98/34/EC, Directive 2004/18/EC].
- [7] EN 1996-1-1 (2006): Eurocode 6: Design of masonry structures - Part 1-1: General rules for reinforced and unreinforced masonry structures.
- [8] Croce P., Holický M. eds. (2013) “Operational methods for the assessment of existing structures”.
http://www.leonardo.cvut.cz/download/march2014/Operational_Methods_for_the_Assessment_of_Existing_Structures.pdf
- [9] Desideri A., Russo G., Viggiani C., *Rivista Italiana di Geotecnica* (n°1 1997), “La stabilità di torri su terreno deformabile”.
- [10] Diamantidis D., Holický M. eds. (2012) “Innovative methods for the assessment of existing structures”. CTU in Prague, Klokner Institute, Prague.
http://www.leonardo.cvut.cz/download/Innovative_Methods_for_the%20Assesstement_of_Existing_Structures.pdf
- [11] Gasperini M., Associazione “Salviamo l’Acquedotto Mediceo” di Pisa (2010), “Progetto preliminare di recupero, valorizzazione e riqualificazione ambientale dell’Acquedotto Mediceo di Pisa e delle sue aree contermini”.
- [12] Giannessi O. (1967), “Si deve salvare l’Acquedotto Mediceo?”, Extracted from the n°9-10 Year III della “Rassegna periodica di informazione del Comune di Pisa”, Tipografia Comunale, Pisa.
- [13] Giuffrè A. (2003), “La meccanica nell’architettura: La Statica”.
- [14] Heyman J. (1997), “The Stone Skeleton: Structural Engineering of Masonry Architecture”.

- [15] Holický M., Návarová V. eds. (2013) “Basics for assessment of existing structures”.
http://www.leonardo.cvut.cz/download/march2014/Basics_Assessment_Existing_Structures_CB.pdf
- [16] Letizia M. G. e Quercioli C. (2007), “Chiare, fresche et dolci acque, C'era una volta l'Acquedotto Mediceo... e le fontane di Pisa”, Musetti Libri, Pisa.
- [17] Zamperini E. (2010), Notes of the Course of Recupero e Conservazione degli edifici, “L'arco in muratura”.

CHAPTER 9 - ANNEX A

MECHANICAL PROPERTIES OF STRUCTURAL MATERIALS

For the different kinds of masonry most often found in structures, the Italian Standard [5], in Table C8A.2.1 shown below (Tab. A.1), provides a range of the reference values for the mechanical parameters.

In the tables the symbols indicate:

- f_m is the average compressive strength of masonry;
- τ_0 is the average shear strength of masonry in absence of compression;
- E is the average value of the modulus of elasticity;
- G is the average value of the shear modulus;
- w is the average specific weight of the masonry.

Table A.1 Reference values of the mechanical parameters and the specific weight - Tab. C8A.2.1 of Italian Standard [5]

Type of masonry:	f_m [kN/m ²]	τ_0 [kN/m ²]	E [N/mm ²]	G [N/mm ²]	w [kN/m ³]
Masonry in disorganized cut stones	1000	20	690	230	19
	1800	32	1050	350	
Masonry with rough-hewed stones, thin skin and internal core	2000	35	1020	340	20
	3000	51	1440	480	
Cut stone masonry	2600	56	1500	500	21
	3800	74	1980	660	
Masonry in pieces of soft stone	1400	28	900	300	16
	2400	42	1260	420	
Masonry in rough-hewed pieces of igneous rock	6000	90	2400	780	22
	8000	120	3200	940	
Full brick and lime mortar	2400	60	1200	400	18
	4000	92	1800	600	
Half-full brick and lime mortar	5000	240	3500	875	15
	8000	320	5600	1400	
Half-full clay block	4000	300	3600	1080	12
	6000	400	5400	1620	
Half-full clay block, with vertical dry mortar joint	3000	100	2700	810	11
	4000	130	3600	1080	
Masonry in concrete block or expanded clay	1500	95	1200	300	12
	2000	125	1600	400	
Masonry in concrete half-full block	3000	180	2400	600	14
	4400	240	3520	880	

For the two types of masonry found in the Aqueduct, the reference values highlighted in the above table have been considered.

The compressive and shear strength have been assumed equal to the minimum values, the elastic and the shear modulus in the uncracked condition equal to the mean values; the elastic modulus in the cracked condition is equal to half the value of modulus for the uncracked condition.

CHAPTER 9 - ANNEX B
ELASTIC RESPONSE SPECTRA

In Italian Standard [4], as well as in Eurocode EN1998-1 [6], the elastic response spectrum of the horizontal component of the acceleration is given by:

$$\begin{aligned}
 0 \leq T < T_B & \quad S_e(T) = a_g \cdot S \cdot \eta \cdot F_o \cdot \left[\frac{T}{T_B} + \frac{1}{\eta \cdot F_o} \left(1 - \frac{T}{T_B} \right) \right] \\
 T_B \leq T < T_C & \quad S_e(T) = a_g \cdot S \cdot \eta \cdot F_o \\
 T_C \leq T < T_D & \quad S_e(T) = a_g \cdot S \cdot \eta \cdot F_o \cdot \left(\frac{T_C}{T} \right) \\
 T_D \leq T & \quad S_e(T) = a_g \cdot S \cdot \eta \cdot F_o \cdot \left(\frac{T_C \cdot T_D}{T^2} \right)
 \end{aligned} \tag{B1}$$

where $S = S_s \cdot S_T \geq 1.0$ depends on soil category and on topography, while T_B , T_C and T_D , expressed in s, are the values of the fundamental period corresponding to the starting points of the constant acceleration branch, of the constant velocity branch and of the constant displacement branch of the elastic response spectrum, respectively. F_o is the factor of the maximum amplification, which in Eurocode is set equal to 2,5 and in Italian Standard assumes different values ($\geq 2,2$) depending on the site.

In eqs. (B1) the coefficient η takes into account the effects of damping coefficient ξ , expressed in percent. The general expression for η is

$$\eta = \sqrt{\frac{10}{5 + \xi}} \geq 0,55 \tag{B2}$$

usually set equal to 1,00.

The elastic response spectrum of the horizontal component of the displacement is defined as:

$$\begin{aligned}
 0 \leq T \leq T_E & \quad S_{De}(T) = S_e(T) \cdot \left(\frac{T}{2\pi} \right)^2 \\
 T_E < T \leq T_F & \quad S_{De}(T) = 0,025 \cdot a_g \cdot S \cdot T_C \cdot T_D \cdot \left[F_o \cdot \eta + (1 - F_o \cdot \eta) \cdot \frac{T - T_E}{T_F - T_E} \right] \\
 T > T_F & \quad S_{De}(T) = 0,025 \cdot a_g \cdot S \cdot T_C \cdot T_D
 \end{aligned} \tag{B3}$$

T_E varies from 4,5s to 6,0s, depending on soil category, and T_F is equal to 10,0s.

CHAPTER 9 - ANNEX C

SEISMIC VERIFICATIONS

The seismic verifications were performed according to Italian Standard [4]. As far as ULS, out of plane failure in shear or bending was checked, while for SLS cracking check has been performed.

Out of Plane Shear Verification (ULS)

At the ULS, the design value of the shear load applied to the masonry wall, V_{Ed} , shall be less than or equal to the design value of the shear resistance of the wall, V_{Rd} :

$$V_{Ed} \leq V_{Rd} \quad (C1)$$

The design value of the shear resistance is given by:

$$V_{Rd} \leq f_{vd} t l_c \quad (C2)$$

with:

$$f_{vd} = f_{vk} / \gamma_M \quad \text{and} \quad f_{vk} = f_{vk0} + 0,4 \sigma_0 \quad (C3)$$

- f_{vd} is the design value of the shear strength of the masonry;
- f_{vk0} , f_{vk} are the characteristic shear strength respectively in absence or in presence of compression stress related to the vertical loads acting on the control section;
- σ_0 is the compression stress related to the vertical loads acting on the control section;
- t is the thickness of the wall;
- l_c is the length of the compressed part of the wall.

Out of Plane Bending Moment Verification (ULS)

At the ULS, the design value of the moment applied to the masonry wall, M_{Ed} , shall be less than or equal to the design value of the moment of resistance of the wall, M_{Rd} , such that:

$$M_{Ed} \leq M_{Rd} \quad (C4)$$

The design value of the lateral moment of resistance of a masonry wall, M_{Rd} , is given by:

$$M_{Rd} = (l \cdot t^2 \cdot \sigma_0 / 2) \cdot (1 - \sigma_0 / 0,85 \cdot f_d) \quad (C5)$$

where:

- l is the length of the wall;
- t is the thickness of the wall;
- σ_0 is the compression stress related to the vertical loads and to the complete section;
- f_d is the design compressive strength of the masonry.

Out of Plane Crack Check (SLS)

Cracking of reinforced masonry walls is prevented when the eccentricity of loads is less than the radius of the central core of inertia. For a rectangular section, in which t is the thickness of the wall, the eccentricity of loads is given by:

$$e = \frac{M_{Ed}}{M_{Rd}} \leq \frac{t}{6} \quad (C6)$$

CHAPTER 9 - ANNEX D

KINEMATIC ANALYSIS

D.1 INTRODUCTION

The modes of damage caused by seismic actions in masonry buildings depend essentially on their structural organization: in case of lacking of efficient connections between the components of the building (walls and floors), the masonry structure does not show a clear global behaviour but rather it is frequent the occurrence of partial collapses, generally corresponding to the loss of equilibrium of portions of the structure, the so called “macro-elements”.

In these circumstances, a global model does not comply with the actual seismic behaviour of the structure, and the seismic assessment must consider also local collapse mechanisms, which are generally less resistant and less ductile than those involving the response of the whole building. The first step of the analysis concerns the identification of the mechanisms that can be activated; for each of them, the kinematic analysis may be performed, aimed to evaluate the seismic actions that activate the mechanism (SLS) and the ones that cause the collapse of the macro-element (ULS).

A masonry wall, subject to earthquake, may exhibit different damage mechanisms, conventionally classified into two basic failure mode categories, depending on the direction of the horizontal forces relatively to the mean plane of the wall:

- 1st failure mode category: the mechanism is activated by seismic forces acting orthogonally to the wall plane, which cause the overturning of a portion or the entire wall (figs. D.1, D.2);
- 2nd failure mode category: the mechanism is activated by seismic forces acting parallel to the wall plane, which usually induce diagonal shear cracks (fig. D.3).

Considering that in case of the aged structures, the mechanisms of the 1st failure mode category take place early during an earthquake, their study is very important, also in view of the design of interventions for improvement and/or seismic retrofitting. The analysis must be performed on a limited number of mechanisms, which are identified as probable to occur, considering the characteristics of the building and/or the crack patterns, eventually induced by an earthquake.



Figure D.1 Overturned tympanum and cracks indicating incipient overturning of the building facade



Figure D.2 Out of plane overturned wall



Figure D.3 Diagonal shear cracks in a masonry wall

D.2 TYPES OF ANALYSIS AND BASIC ASSUMPTIONS

Local mechanisms which may occur in the masonry walls can be studied by means of the kinematic analysis, which allows to determine the variation of the horizontal action that the structure is able to withstand as the mechanism develops. The kinematic analysis is based on the kinematic theorem of the limit analysis method. According to the kinematic approach, the application of virtual works theorem allows to estimate the load multiplier corresponding to the activation of the local mechanisms (damage limit state) and to the collapse (ultimate limit state).

Generally, two different kind of analysis are foreseen:

- Linear kinematic analysis, leading to the definition of the load multiplier, or the peak ground acceleration (PGA), activating the local mechanism;
- Non-linear kinematic analysis, leading to the definition of the local displacement corresponding to the local collapse.

For each significant local failure mode identified, the following procedure should be applied:

- *transformation of a part of the building in a mechanism (kinematic chain)*, through the identification of rigid bodies, delimited by the fracture planes and able to rotate or slide relative to one another according the damage and collapse mechanisms;
- *assessment of the α_o loads multiplier* corresponding to the mechanism activation (damage limit state);
- *assessment of the evolution of horizontal loads multiplier α* until the annulment of the horizontal seismic force, as a function of the increase of the displacement d_k of a suitable control point of the kinematic chain, point that is usually chosen close to the center of gravity of the considered part;
- *transformation of the curve so obtained in a capacity curve*, expressing the relationship between the spectral acceleration a^* and the spectral displacement d^* , and evaluation of the ultimate displacement, corresponding to failure (ultimate limit state);
- *safety assessment*, by controlling the compatibility of displacements and/or strengths required by the analysis with those offered by the structure.

The method applied is essentially based on the Heyman model [14], that is on the following assumptions:

- masonry tensile strength equal to zero;
- lack of sliding between the blocks;
- infinite masonry compressive strength.

However, in many cases, in order to arrive to a more realistic simulation of the actual behaviour, it is appropriate to improve the model taking under consideration, at least in an approximate form:

- the sliding between the blocks, considering the friction presence;
- the connections, also of limited strength, between the masonry walls;
- the presence of metal chains;
- the limited masonry compressive strength, considering the hinges set back with respect to the edge of the section;
- the presence of disconnected wall facades.

D.3 LINEAR KINEMATIC ANALYSIS

The linear kinematic analysis consists in the evaluation of the α_0 load multiplier that determines the local damage mechanism activation and it is mainly used to assess serviceability limit states (SLS).

Each macro-element is considered as a kinematic chain, composed of rigid blocks, connected by hinges (fig. D.3).

The following systems of forces must be taken into account:

- a system of vertical forces W_i and P_j , being W_i the weight of i -th masonry block, applied in its centroid, and P_j the vertical loads transmitted to the blocks by floors, roofs, vaults and other masonry elements not considered in the structural model;
- a system of horizontal forces, proportional through α to the vertical loads carried by each block, provided that they are not effectively transmitted to other parts of the building;
- internal horizontal forces Q_k transmitted by structural elements, like the thrusts of arches, domes and vaults;
- horizontal component of stabilizing external forces F_h , such as those transmitted by metal chains or FRP tie, or stabilizing internal forces, like those offered by the connections with adjacent walls.

The kinematic multiplier can be evaluated using the Virtual Work Theorem.

Assigned a virtual rotation θ_i to the i -th masonry block, the virtual displacements δ associated with it can be easily determined as a function of the geometry of the structure.

The multiplier α_0 is obtained by applying the Principle of Virtual Work, in terms of displacements, equalling the total work performed by the external and internal forces applied to the system at the act of virtual motion:

$$\alpha_0 \left(\sum_i W_i \delta_{xi} + \sum_j P_j \delta_{xj} \right) + \sum_k Q_k \delta_{xk} - \sum_i W_i \delta_{yi} - \sum_j P_j \delta_{yj} - \sum_n F_h \delta_{xn} = L_{fi} \quad (D1)$$

where δ_x are the virtual displacements of the horizontal forces, δ_y are the virtual displacements of the vertical forces and L_{fi} the virtual works of other internal forces.

D.4 NON-LINEAR KINEMATIC ANALYSIS

The non-linear kinematic analysis is devoted to investigate the displacement capacity of the structure when the collapse occurs through the considered mechanism.

The horizontal load multiplier α can be calculated not only on the initial configuration, as described above for linear analysis, but also on the macro-element displaced configurations: in this way, the evolution of the mechanism can be exhaustively defined, through a relationship $\alpha = \alpha(d_k)$ linking the load multiplier α with the displacement d_k of a control point of the macro-element, as explained in C8A.4 of Italian Standard [5]. The analysis will be terminated when the load multiplier becomes zero; the correspondent displacement of the control point $d_{k,0}$ is representative of the collapse situation.

The relationship $\alpha = \alpha(d_k)$ can be obtained analytically, graphically or numerically, applying the Virtual Work Theorem in the deformed configurations, and considering the effect of the displacements on the load configuration.

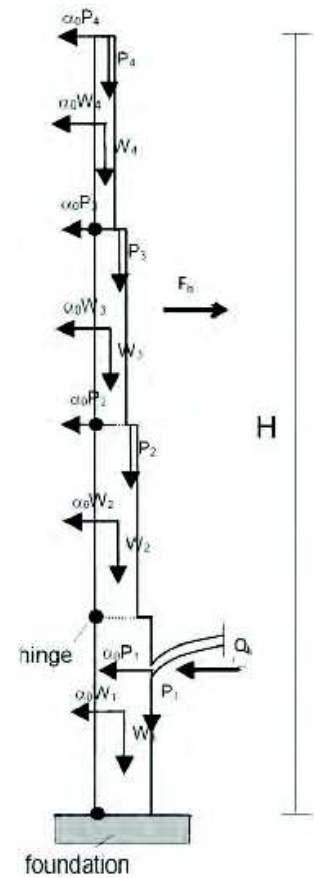


Figure D.4 Kinematic analysis of a macro-element

If the forces (weight forces, external or internal force) are not depending on the displacement, the $\alpha=\alpha(d_k)$ curve can be approximated by a straight line expressed by:

$$\alpha = \alpha_0 \left(1 - \frac{d_k}{d_{k,0}} \right) \quad (D2)$$

where: α and d_k are the load multiplier and the corresponding displacement in a generic displaced configuration; α_0 can be derived from linear kinematic analysis and $d_{k,0}$ from non-linear analysis in correspondence of $\alpha=0$.

D.5 CAPACITY CURVE

From the relationship $\alpha = \alpha(d_k)$ may be derived the capacity curve of the equivalent simple oscillator, in terms of acceleration a^* and displacement d^* .

The participating mass M^* can be estimated considering the virtual displacements of the points of the macro-elements as a simplified representation of its fundamental mode shape, so that it results:

$$M^* = \frac{\left(\sum_i W_i \delta_{xi} + \sum_j P_j \delta_{xj} \right)^2}{g \left(\sum_i W_i \delta_{xi}^2 + \sum_j P_j \delta_{xj}^2 \right)} \quad (D3)$$

where the sums are extended to all the applied weights W_i and vertical loads P_j associated with the macro-element under examination.

From (D1) and (D2), it can be determined the spectral acceleration a^* :

$$a^* = \frac{\alpha \left(\sum_i W_i + \sum_j P_j \right)}{M^*} \quad (D4)$$

In particular, introducing α_0 , we can obtain the spectral acceleration a_0^* which can be seen as the acceleration to be applied to the participating mass M^* to obtain the horizontal inertia forces activating the mechanism. In other words, a_0^* is the maximum spectral acceleration to which the macro-element can resist before the mechanism activation.

The spectral displacement d^* of the equivalent oscillator may be evaluated as the weighted average of the displacements of the points where the weights are applied. Approximately, we can define d^* on the base of the virtual displacements in the initial configuration:

$$d^* = d_k \frac{\sum_i W_i \delta_{xi}^2 + \sum_j P_j \delta_{xj}^2}{\delta_{x,k} \left(\sum_i W_i \delta_{xi} + \sum_j P_j \delta_{xj} \right)} \quad (D5)$$

where $\delta_{x,k}$ is the virtual horizontal displacement of the control point and the other symbols have been defined above.

When the curve may be approximated by a straight line, the capacity curve assumes the following expression:

$$a^* = a_0^* \left(1 - \frac{d^*}{d_0^*} \right) \quad (D6)$$

where d_0^* is the spectral displacement corresponding to $d_{k,0}$.

The resistance and the displacement capacity related to the SLS and ULS are derived from the capacity curve, at the following points:

- SLS: spectral acceleration a_0^* , corresponding to the activation of the mechanism;
- ULS: spectral displacement d_u^* , equal to the smaller between:
 - the 40% of d_0^*
 - the displacement corresponding to local situation inconsistent with the stability of the construction elements (i.e. fall of the beams).

D.6 SAFETY VERIFICATIONS

Serviceability Limit State

The safety verification SLS is satisfied when spectral acceleration corresponding to the activation of the mechanism, a_0^* , is higher than the acceleration demand.

In case of verifying an element placed directly on the ground, the acceleration demand is the peak ground acceleration, i.e. the spectral acceleration for $T=0$:

$$a_0^* \geq a_g(P_{VR}) \cdot S \quad (D7)$$

where:

a_g is the peak ground acceleration of the site for the given probability of exceeding, P_{VR} [4]

S is the subsoil coefficient [4].

In the case that the local mechanism affects a portion of the building situated at a certain height, the amplification of the acceleration must be taken into account, so:

$$a_0^* \geq S_e(T_1) \cdot \psi(Z) \cdot \gamma \quad (D8)$$

where:

$S_e(T_1)$ is the value of the elastic response spectrum corresponding to the fundamental period T_1 of the entire structure in the direction of the mechanism, $\psi(Z)$ is the amplitude of the mode shape, normalized with respect to the maximum mode shape amplitude, at the height Z of the constraints between the blocks involved in the mechanism and the rest of the structure, γ is the corresponding modal mass participation factor.

Ultimate Limit State

The safety verification of the local mechanism in the Ultimate Limit State consists of comparing the capacity spectral displacement d_u^* , as defined above, with the displacement demand obtained from the displacement spectrum for the secant period T_s :

$$T_s = 2\pi \sqrt{\frac{d_s^*}{a_s^*}} \quad (D9)$$

where:

$$d_s^* = 0,4 \cdot d_u^* \quad (D10)$$

a_s^* is the acceleration corresponding to d_s^* in the capacity curve.

When assessing an element placed directly on the ground, the check is satisfied when:

$$d_u^* \geq S_{De}(T_s) \quad (D11)$$

where $S_{De}(T_s)$ is the displacement elastic response spectrum.

In the case that the local mechanism affects a portion of the building situated at a certain height, the displacement elastic spectrum at the height of the portion involved in the mechanism must be considered; approximately:

$$d_u^* \geq S_{De}(T_1) \cdot \psi(Z) \cdot \gamma \cdot \frac{\left(\frac{T_s}{T_1}\right)^2}{\sqrt{\left(1 - \frac{T_s}{T_1}\right)^2 + 0,02 \frac{T_s}{T_1}}} \quad (D12)$$

CHAPTER 9 - ANNEX E

EVALUATION OF SOIL-STRUCTURE INTERACTION AND SECOND ORDER EFFECTS

The out-of-plane capacity curve of the studied system (masonry element and foundation + interacting soil) was studied taking into account the mechanical characteristics of the masonry and of four different layers of soil, and the second order effects due to bending induced by self weight acting eccentrically as a consequence of the horizontal displacements of the layers.

The method applied is the iterative method of *Finite Differences*.

The studied system was previously subdivided in several layers, each characterized by its own cross section, mechanical properties and compression force, N . For each layer, the moment-curvature diagram was calculated.

E.1 MOMENT-CURVATURE DIAGRAMS

The relationship between moment and curvature has been evaluated by a step-by-step procedure, in the following hypotheses:

- the principle of conservation of plane sections is valid;
- the materials are no-tension;
- the behaviour of the materials is elastic-perfectly plastic;
- the value of normal force, N , is constant for each layer.

For each value of the curvature of the section, χ , the vertical deformation of the centroid of the section, $\varepsilon_G^{(1)}$, is arbitrarily fixed; by this way, the neutral axis, and, by means of the constitutive law, the stress diagram and the resultant force, $N^{(1)}$, are determined. If the value of $N^{(1)}$ is not sufficiently close to the value of N really acting on the section, the procedure is repeated, changing appropriately the tentative value of ε_G , according to the *Newton-Raphson* algorithm.

When the requested approximation is reached, the value of $N^{(i)}$ satisfies the translational equilibrium; the corresponding value of the eccentricity allows to calculate M , i.e. the value corresponding to χ in the moment-curvature diagram. The procedure is repeated for a discrete series of values of χ ; so the diagram is built by segments.

For the case under examination, the curves to be determined are sixteen, one for each layer, taking into account the dimensions and vertical load acting on each of them. fig. E.1 shows the diagram found for the layer at the base of the pillar.

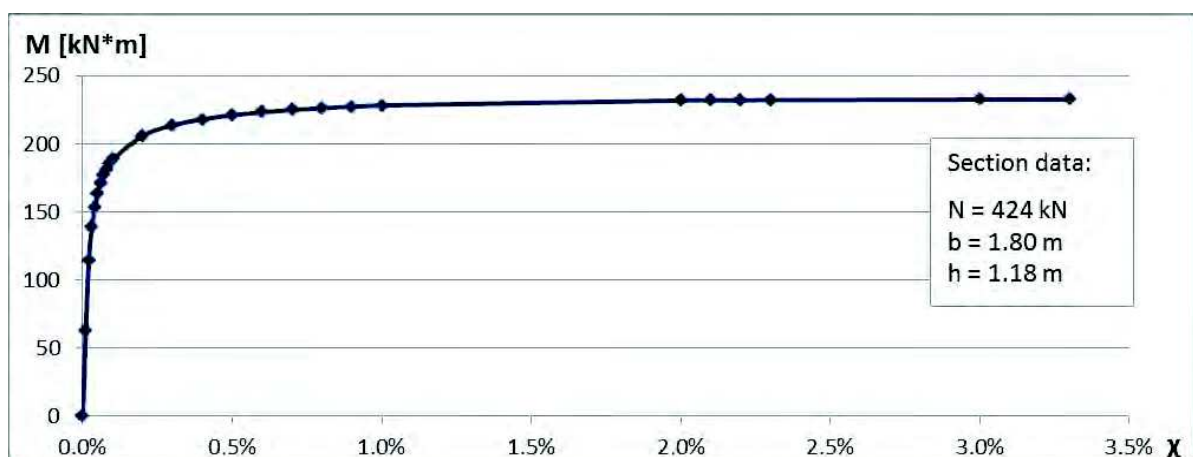


Figure E.1 Moment-curvature diagram corresponding to masonry section n°10

E.2 CALCULATION OF THE DEFORMED CONFIGURATION

Consider the model described in §4.4.5: each layer of the element is subjected to the corresponding self-weight and to a lateral force, F_i , simulating the seismic action; lateral forces are equal to the product of the mass of the layer for its height related to the extrados of the foundation, and for the acceleration of soil, a . The deformed configuration, considering the second order effects, is evaluated by a step-by-step procedure based on the *Finite Differences* method.

The general equation of *Finite Differences* expresses the displacement, y_n , of the n -th section according to the Taylor series, stopped to the third term:

$$y_n = y_{n-1} + q_n \cdot y'_{n-1} + \frac{q_n^2}{2} \cdot y''_{n-1} \quad (\text{E1})$$

where:

- q_n is the distance between n -th and $(n-1)$ -th sections.

Assuming that approximately y''_{n-1} is equal to the curvature of the section

$$y''_{n-1} = \chi_{n-1} \quad (\text{E2})$$

and that approximately:

$$y'_{n-1} = \frac{y_n - y_{n-2}}{q_n + q_{n-1}} \quad (\text{E3})$$

the general equation becomes:

$$y_n = \frac{q_{n-1} + q_n}{q_{n-1}} \cdot \left[y_{n-1} - \frac{q_n}{q_{n-1} + q_n} \cdot y_{n-2} + \frac{q_n^2}{2} \cdot \chi_{n-1} \right] \quad (\text{E4})$$

In the case study, such equations can be written for each layer, allowing to evaluate the horizontal displacement of the centroid of the layers. Initially, for each layer the first order moments are considered and the correspondent values of the curvature, χ , are obtained from the appropriate moment-curvature diagram. Using the equation (E4), the values of the horizontal displacements of the centroid of each layer, y_n , are calculated. At the next steps, the second order moments are considered too. When the displacement of the top section differs less than 10^{-6} m from that found in the previous step, the operation stops and the actual deformed configuration is found.

In fig. E.2 are shown the deformed configurations at each step of the procedure for a given set of lateral forces F_i , i.e. a given value of a .

In fig. E.3 are shown the final deformed configurations related to six different values of a .

E.3 DETERMINATION OF THE CAPACITY CURVE

The procedure described in §E.2 is applied for increasing values of the horizontal acceleration, a , obtaining the corresponding displacements, d , of the control point, placed in the centroid of the key section. The procedure stops when, in a certain layer, the resisting moment is reached, so that, also for little increments of the moment, the curvature increases very much and the procedure does not converge. The method allows to identify the critical section, in which the failure occurs.

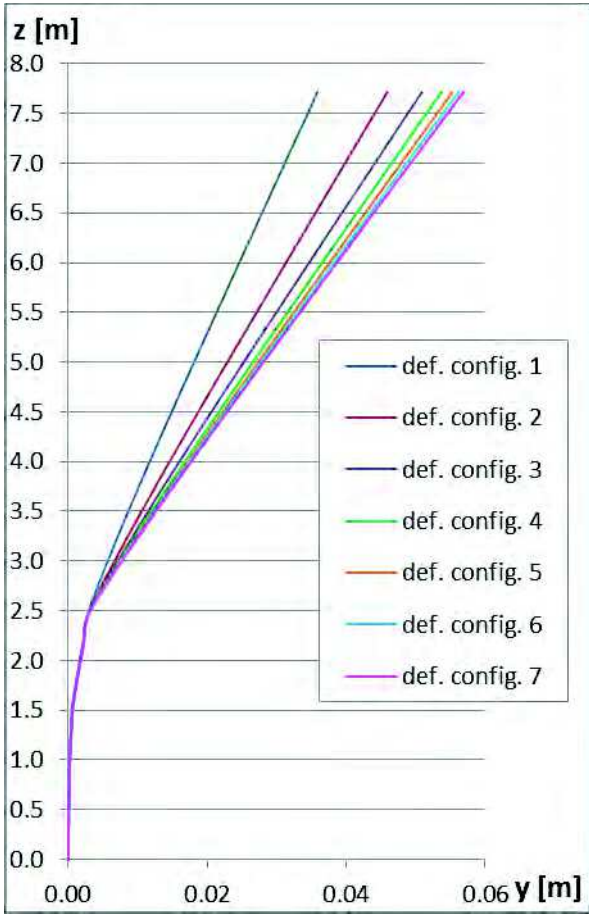


Figure E.2 Deformed configurations at each step for $a = 1,17 \text{ m/s}^2$

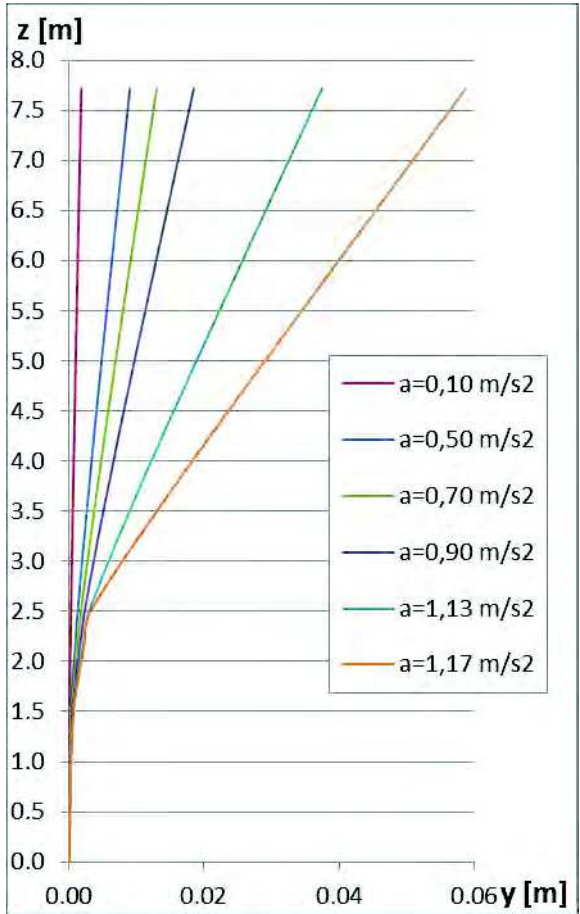


Figure E.3 Final deformed configurations corresponding to different values of a

CHAPTER 9 - ANNEX F

EVALUATION OF STABILIZING FORCES

In fig. F.1 a plan view of the arches, in which each block corresponds to a macro-element separated from the others in correspondence of the arch keys. Due to the out-of-plane rotation at the pillar's foot, the top of the macro-element moves transversely by δ . In the fig. F.1 only half of the interesting portion is represented, given the symmetry of the configuration.

As described in §4.5.2 a sort of arch effect may develop in the horizontal plane; so a compressed band takes place, as indicated by the area highlighted in grey.

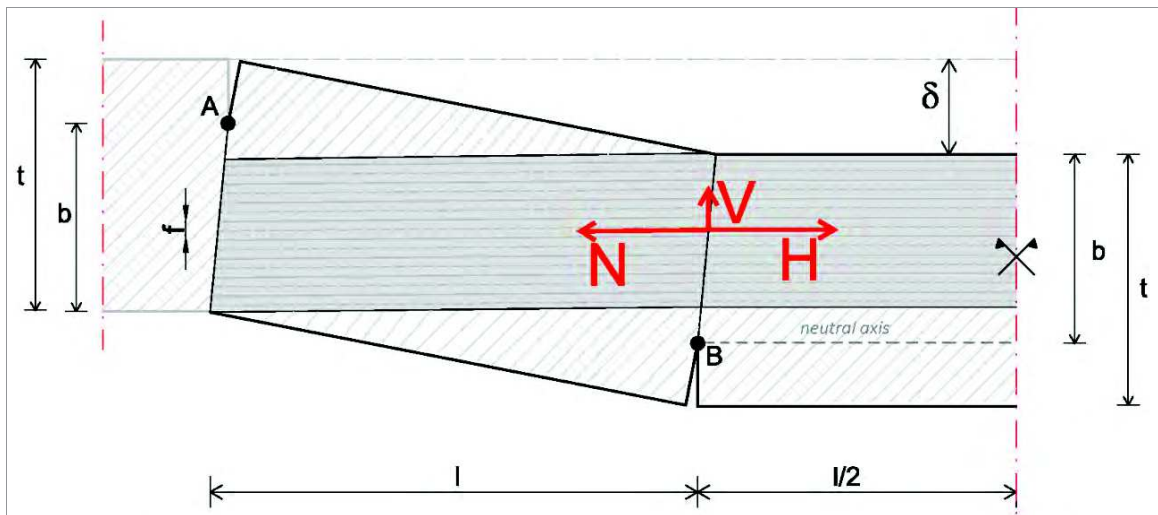


Figure F.1 The arch mechanism

The relationship between the force V acting between the macro-elements at the interface and the displacement δ , may be evaluated assuming the following hypotheses:

- 1) stress-block constitutive law for masonry;
- 2) the deformations are assumed to be zero in the external hinges of the constraint sections ($\epsilon(A) = 0$, $\epsilon(B) = 0$); as a consequence, the line BB' , representing the neutral axis, have constant length;
- 3) the level of stress is assumed to be the same in the constraint sections; therefore, in both sections, the depth of the neutral axis is equal to “ b ”.

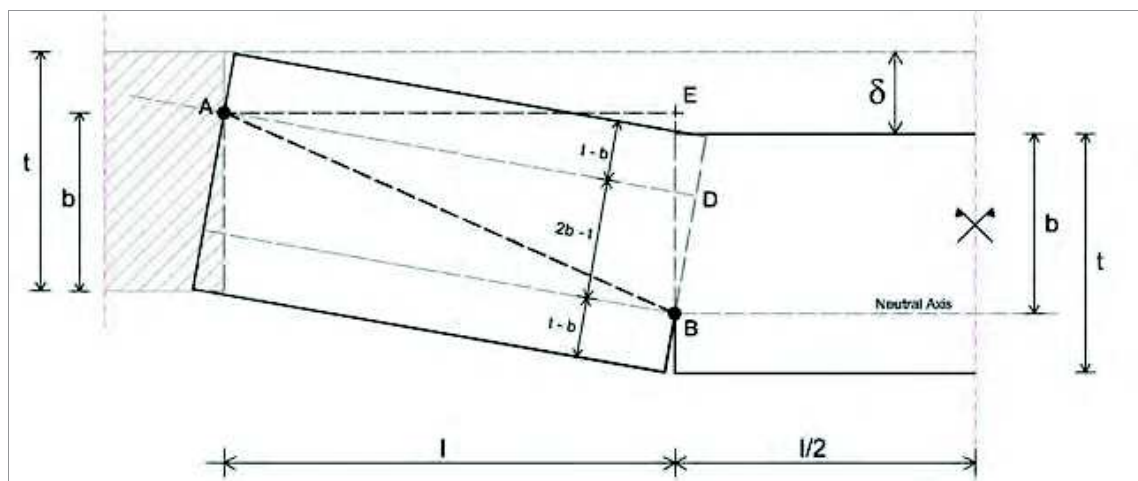


Figure F.2 The arch mechanism

Referring to fig. F.2:

$$\overline{BD} = |t - 2(t - b)| = |2b - t| \quad (\text{F1})$$

$$\overline{AD} = \overline{AE} = l \quad (\text{F2})$$

$$\overline{AB} = \sqrt{l^2 + (2b - t)^2} \quad (\text{F3})$$

$$\overline{EB} = b + \delta - (t - b) = \delta + 2b - t \quad (\text{F4})$$

Considering:

$$\overline{AE}^2 = \overline{AB}^2 - \overline{EB}^2 \quad (\text{F5})$$

$$l^2 = l^2 + (2b - t)^2 - (\delta + 2b - t)^2 \quad (\text{F6})$$

which yields the congruence condition:

$$b = \frac{t}{2} - \frac{\delta}{4} \quad (\text{F7})$$

At the constraint sections, considering a stress-block distribution of tension, the resultant of the compressions is:

$$N = 0,8bsf_m = 0,4\left(t - \frac{\delta}{2}\right)sf_m \quad (\text{F8})$$

where f_m is the compressive strength of the masonry.

Referring to fig. F.1:

$$f = (t - 0,4b) - (0,4b + \delta) = t - 0,8b - \delta \quad (\text{F9})$$

$$H = \frac{VL}{f} \quad (\text{F10})$$

$$N = \sqrt{H^2 + V^2} = V\sqrt{1 + \frac{l^2}{f^2}} \quad (\text{F11})$$

Equating (F8) and (F11), we obtain:

$$0,4\left(t - \frac{\delta}{2}\right)sf_m = V\sqrt{1 + \frac{l^2}{f^2}} \quad (\text{F12})$$

Finally, combining (F7), (F9) and (F12):

$$V(\delta) = \frac{0,04f_mst\left(2 - \frac{\delta}{t}\right)\left(3 - 4\frac{\delta}{t}\right)}{\sqrt{\left(0,6 - 0,8\frac{\delta}{t}\right)^2 + \left(\frac{l}{t}\right)^2}} \quad (\text{F13})$$

Expression (F13) leads to a diagram like that shown in fig. 67 §4.5.2.

It must be noted that, for small values of δ , the compressive force is small, so that the hypothesis of the stress block is not valid. In this case expression (F13) is supposed to be valid for δ greater than the displacement δ_e that determines the achievement of the elastic limit deformation in the most stressed fibre of the arch mechanism.

To preserve the smoothness of the curve itself, the first part of the diagram has been fitted with a cubic curve, passing from the origin, tangent to the curve determined as described above at the point δ_e and characterized by a decreasing slope in the left neighbourhood of δ_e itself, so obtaining the diagram illustrated in fig. 67 (§4.5.2).